UNIVERSITÀ DEGLI STUDI DI TRIESTE

Sede Amministrativa del Dottorato di Ricerca

Electrolux Italia S.p.a. - C.T.I. (Cross Technology and Innovation)

DOTTORATO DI RICERCA

INGEGNERIA E SCIENZA DEI MATERIALI

XXI CICLO

A NOVEL APPROACH TO THE EXPERIMENTAL STUDY OF THERMOPLASTIC COMPOSITES FATIGUE BEHAVIOUR

(Settore Scientifico Disciplinare Ing – Ind / 22)

Dottorando

Dott. Ing. **ANDREA CREVATIN**

Coordinatore Collegio Docenti e Relatore

Prof. **SERGIO MERIANI**

Tutore

Dott. Ing. **FABIO SPIZZO**

Correlatore

Dott. Ing. **MONICA CELOTTO**

ANNO ACCADEMICO 2007 - 2008

Contents

Introduction

Nowadays most industrial realities undergo a strong push to improve cost-effectiveness, productivity and quality of manufactured products. In particular we focussed our attention in the area of design of plastic structural components, including both optimization of existing structures and design of new ones. In this case, but the following considerations have a more general value, these needs could be translated into demanding requirements of cost-effectiveness, weight reduction, reduced time-to-market with guarantee reliability. From a material perspective this means demanding mechanical performances, attention to safety margins and need of a better control of key design parameters. To obtain these results, we need to develop a new approach and effective tools in the design of plastic materials and component aimed at tailoring part behaviour to endurance and performance requirements.

The target of the project is to find effective tools for predicting life endurance and damage evolution of plastic materials and components under mechanical/thermal service loading, in order to support the development of new material formulations and the design and optimization of structural components.

In a particular way, we focussed our work on the characterization and modellization of materials durability and damage mechanisms.

One of the main problems related to materials durability is due to fatigue failure. Fatigue process is a progressive weakening of a component with increasing time under load such that loads to be supported satisfactorily for short duration produce failure after long durations. Fatigue failure should not be thought only as the breaking of the specimen into two separated pieces, but as a progressive material damage accumulation. Material damage during fatigue loading manifests as progressive reduction of stiffness and as creep.

As standard fatigue testing is expensive in terms of money and time, it is essential to develop new approaches less time consuming and simpler to be implemented. One of the most important goals of the present work is the setting of an investigation method (Accelerated Fatigue Test) very simple to be implemented that is able to differentiate damage accumulation and durability performances of various material formulations in reduced time.

Furthermore we have tried to simulate the results obtained with the AFT method by following two approaches, a mechanical one, by the development of a constitutive mathematical model, and a systemic one, by the development of a neural network.

As a final step of the work, the data of the AFT method have been correlated with the performances of a structural component in service conditions. The stress mapping of the component has been measured by the strain gauging technique.

1

Introduction to fatigue

The aim of this chapter is to give an overview of the actual state-of-the-art about fatigue performances of polymer composites, mainly focussed on PP-based formulations. The basics mechanisms regulating the fatigue behaviour of these materials are described together with the most common design approaches followed for a durability-focussed design of plastic components.

The review comprises the following aspects:

- available design criteria for the prediction of life endurance;
- non-destructive techniques to assess damage evolution and defects propagation on parts/materials subjected to service conditions and life tests;
- different fatigue analysis approaches for a durability-focussed design, their advantages and limitations;
- fatigue damage mechanisms, role of material formulation and of working conditions;

1.1 Life Estimation Philosophies

Before attempting to carry out a fatigue calculation, or even choosing a way of doing that calculation, it is necessary to decide on a design philosophy.

The main differences among different design philosophies often rest on how the crack initiation and the crack propagation stages of fatigue are quantitatively treated.

The three main approaches are: *Safe-Life*, *Fail-Safe* and *Damage-Tolerant* [1].

1.1.1 Safe-Life

In the *Safe-Life philosophy*, products are designed to survive a specific design life with a chosen reserve. The design life will be some fraction of the estimated life, typically about one fifth for safety-critical components. The penalty is that components have to be taken out of service when it is likely than they still have substantial remaining life.

1.1.2 Fail-Safe

Fail-Safe philosophy may be adopted to maintain or improve the operating safety of a component in the later stage of its life. This philosophy is based on the argument that, even if an individual member of a large structure fails, there should be sufficient structural integrity in the remaining parts to enable the structure to operate safely until the crack is detected. Component which have multiple load paths, are generally fail-safe because

of structural redundancy. An inspection procedure to detect the failure is needed and a clear definition of action to be taken following this inspection must be specified.

1.1.3 Damage-Tolerant

A design procedure based on the *Damage-Tolerant philosophy* needs a close understanding of how cracks grow steadily under varying loads and extend catastrophically when they reach a certain length. It is important to note that, when using this approach, a clearly defined inspection procedure and agreed action following the result of this inspection is required. From a certain point of view, the Damage-Tolerant philosophy can be considered an upgrade of the Fail-Safe one, for components without structural redundancy.

1.1.4 Integrated Durability Management

In the design and development of a large system, more than one of the above approaches may be used in different parts of the system. Coordination on effort is then needed. The overall process is often called Integrated Durability Management. This implies that design, testing and production are coordinated to ensure that products are developed to meet the required life within cost and on time.

1.2 Life Prediction Methods

Classical approaches to fatigue design involve the characterization of total fatigue life to failure, in terms of the cyclic stress range or the strain range. In these methods, the number of stress or strain cycles necessary to induce fatigue failure in initially uncracked laboratory specimens is estimated under controlled amplitudes of cyclic stresses or strains. The resulting fatigue life incorporates the number of fatigue cycles to initiate a dominant crack and to propagate this dominant flaw until catastrophic failure occurs.

According to this view, total life is made up of two stages: a crack initiation phase and a crack propagation phase. The portion of each contribute will vary with the specimen geometry, the loading conditions and especially with the material characteristics.

Various techniques are available to account for the effects of mean stress, stress concentrations, environmental conditions, multiaxial stresses and variable amplitude stress fluctuations in the prediction of total fatigue life using the classical approaches.

In this section the three main life prediction methods are described: Stress-Life, Strain-Life and Crack Propagation Models [2, 3].

One of the problems usually encountered in design for long-term exposure is the high scatter generally affecting fatigue tests. This calls for a better understanding of the causes of variability of fatigue life, as well as for design methods based on statistical approaches [4].

1.2.1 Stress-Life (or S-N) Approach

This approach assumes that all stresses in the component, even the local ones, stay below the elastic limit at all times. It is the oldest method for fatigue analysis and it is suitable when the applied stress is nominally within the elastic range of the material. For this reason this approach is only applicable to high cycle fatigue (HCF) problems. In fact this method doesn't work well in low cycle fatigue (LCF) problems, where the applied strains have a significant plastic component.

Stress cycles

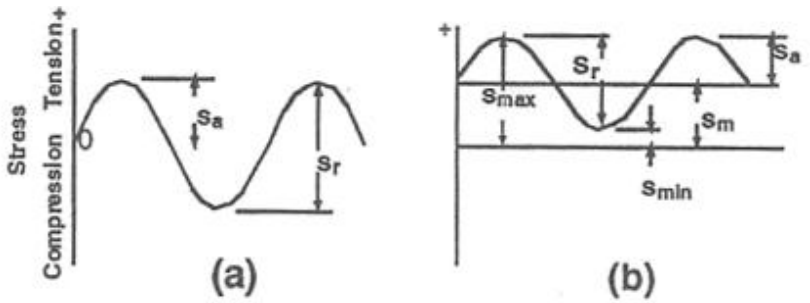

Fig 1.1

Figure 1.1 (a) shows a fully reversed stress cycle with a sinusoidal form (the most common, other forms are also possible such as triangular or square). The maximum and minimum stresses are of equal magnitude, but opposite sign, tensile stress being considered positive and compressive stress negative. Fig. 1.1 (b) illustrates the more general situation where the

maximum and minimum stresses are not equal in magnitude. In this case they are both tensile and so define an offset for the cyclic loading. It is therefore convenient to define a fluctuating stress cycle by two components, a static or mean state stress S_m, and an alternating stress amplitude S_a. It is sometimes necessary to consider the stress range, which is the algebraic difference between the maximum stress in a cycle, S_{max}, and the minimum, S_{min}. The same information can be conveyed by specifying either S_{max} or S_{min} and the stress ratio R, which is S_{min} / S_{max}. R typically varies from -1 (symmetric alternating fatigue) to 1 (pure creep).

Different loading conditions (stress amplitude, mean stress, stress ratio) result in different dominating failure mechanisms (figure 1.2): brittle failure, thermal failure or creep. High stress amplitudes promote thermal failures; brittle failure is instead favoured by low stress amplitude and mean stress; high mean stresses and stress ratios approaching unit favour creep.

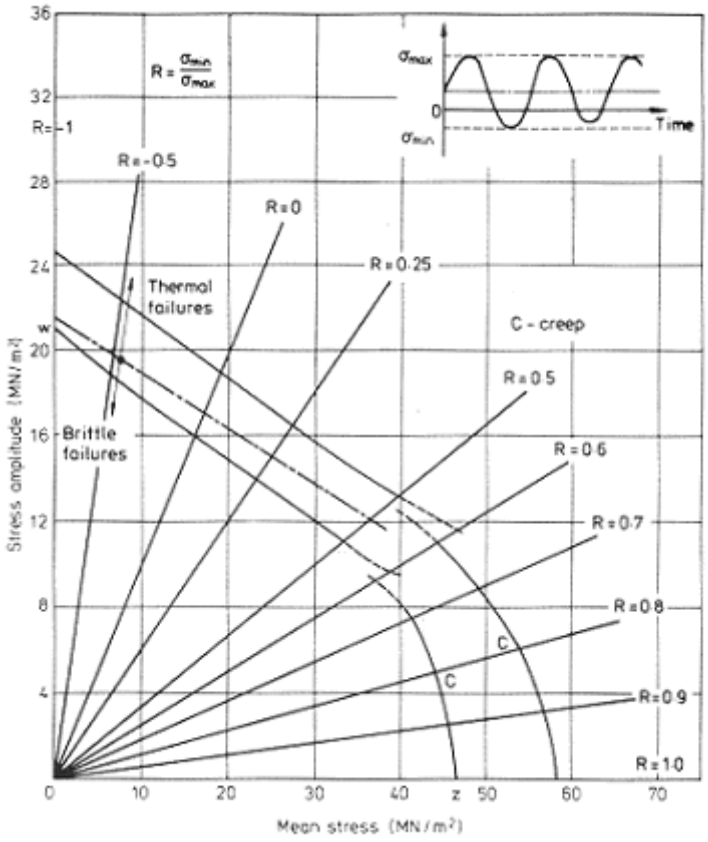

Fig 1.2: relationship between stress amplitude and mean stress

The S-N curve

The Wöhler (or S-N) test is carried out with the following procedure. A specimen with very slow changes of section is cyclically loaded in bending or in axial tension. A number of identical specimens are tested to total break and the number of cycles needed is recorded as *N*. Load, not stress, is controlled during the test. For each specimen various maximum loads are tested, S, and the corresponding number of life cycles (N) for each loading condition are plotted as the un-notched S-N diagram.

The mean line in the finite-life region (10000 to 10 million cycles) is then usually straight in a log-log diagram, giving the Basquin relationship:

$$N = aS^{-b}$$

The inverse slope of the line is b, called the Basquin exponent, and *a* is related to the intercept on the y axis.

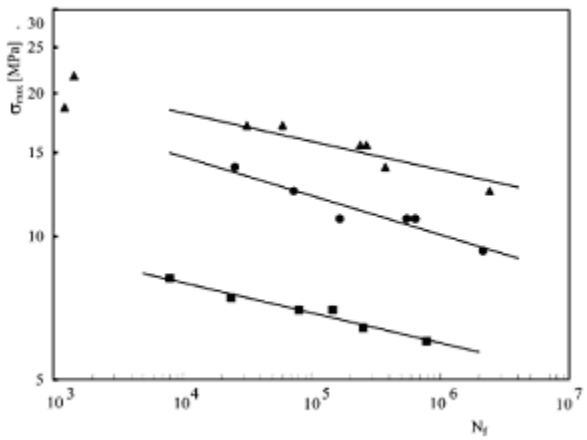

Fig 1.3: Typical Wöhler (or S-N) curves for three different PMMA-based materials

Limit of the S-N Curve

The S-N approach is applicable to situations where all stresses, even local ones, remain in the elastic field. In practice, this means that the S-N curve should be confined on the life axis to numbers greater than about 10^3-10^4 cycles.

The Role of Stress Concentration

Real components have geometrical factors which will cause local "hot spots" of high stress. Fatigue will start at these hot spots and life calculation must allow for their effect.

A way could be converting applied loading into local stresses at the point where crack is likely to start, using a key factor: *stress concentration factor* K_T defined as

K_T = *Maximum stress in the region of the notch / Nominal stress remote from the notch*

Progressive Material Damage during Fatigue Testing

Each loading-unloading cycle during the dynamic loading of the material in the load-controlled fatigue test is characterised by a stress-strain hysteresis loop similar to that schematically reported in figure 4. The area of the loop represents the mechanical work done during the loading-unloading cycle. Part of this work is spent in irreversible processes, resulting in the formation of microscopic deformations as crazes, shear bands, voids and microcracks [5]. The remaining part transforms into heat and contributes to thermal softening.

For polymeric materials, as the fatigue experiment proceeds the hysteresis loops typically shift towards higher displacement values and their average slope is reduced (figure 1.5), as a result of both increased specimens compliance due to the crack propagation and matrix softening due to temperature increase (progressive material damage).

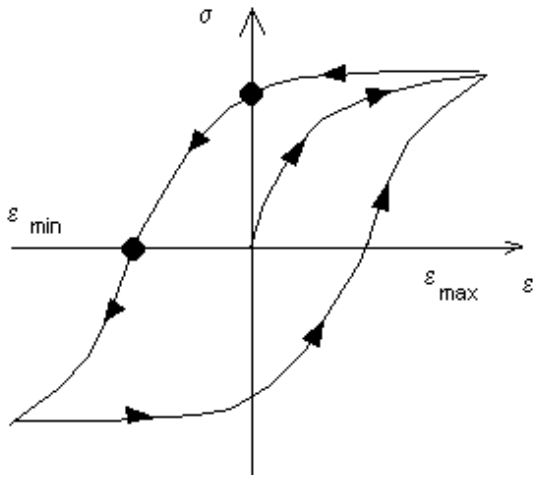

Fig 1.4: Cyclic stress-strain hysteresis loop

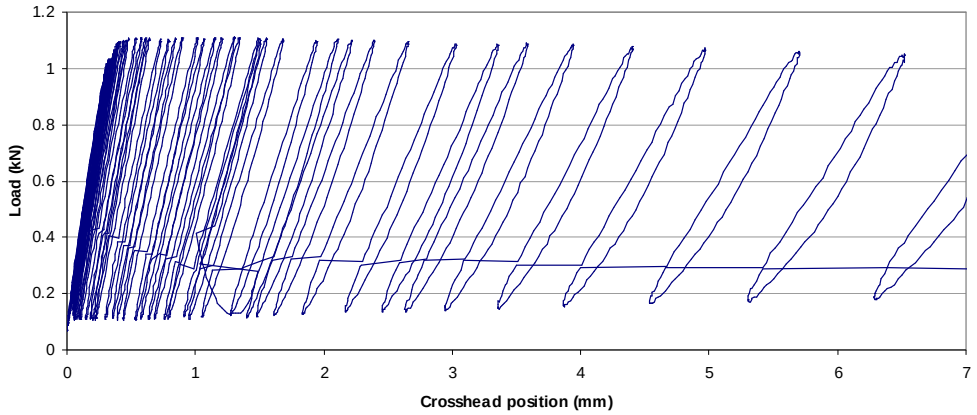

Fig 1.5: Typical progressive deformation of the hysteresis loop during load-controlled fatigue testing

The progressive shift of the hysteresis loops towards higher deformation values corresponds to a creep phenomenon overlapping pure fatigue mechanisms (it is particular evident for large R).

This progressive creep can be followed monitoring cycle after cycle the minimum and maximum elongations of the fatigued specimens (ε_{min}, ε_{max} in figure 1.4). The progressive increase of material compliance can be instead followed monitoring the secant modulus.

When during a fatigue test of a polymeric material with both tension and compression loads the shape of the hysteresis loop remains elliptic with the side relative to the tensile load symmetric with respect to the side relative to compressive loads, the dominating damage mechanism for the material is through shear bands, without any volume variation. When the hysteresis loop becomes irregular, with a higher increase of the tensile area with respect of the compressive area, the dominating damage mechanism for the material is crazing, which is accompanied by volume and tensile compliance increase [2].

Variable Amplitude Tests

Constant amplitude load-controlled fatigue tests are the most common. In real situations anyway fatigue loading conditions often presents variable amplitude cyclic loads. In this case various damage accumulation criteria are available for life prediction under variable amplitude loading histories using fatigue data obtained only in constant amplitude conditions. One of the most used criterion is the Miner's rule [3]. According to this rule, failure occurs when the accumulated fatigue damage reaches unit:

$$D = \sum_{i=1}^{k} \frac{n_i}{N_i} = 1$$

where D is the damage sum, n_i is the number of cycles applied at a stress range of $\Delta\sigma_i$ and N_i is the corresponding number of cycles to failure under constant amplitude tests. The value of N_i is estimated according to the constant amplitude S-N curves. Other approaches are available [3] since the Miner's approach in many cases leads to non conservative life predictions. In

fact it does not take into account the effect of load sequence on the accumulation of damage due to cyclic fatigue loading.

1.2.2 Strain-Life (ε-N) Approach

Modern observations about the mechanism of fatigue damage, show that fatigue is strain (and not stress) controlled. In fact, if we consider a plate with a hole loaded in tension, we see that, although the material remote from the hole stay elastic, the material in the most highly stressed region yields. The plastic deformation associated with this yielding will be the primary cause of fatigue and following its accumulation as the loading history proceeds is likely to give an accurate life prediction.

In the most common situation yielding only occurs in a small region at the root of a notch. The surrounding region remains elastic and when the applied load is removed, the yield zone return to its former shape. This means that the material, forced back to its former shape, does not necessary return to zero stress.

A strain based approach, which accounts for plasticity, must be adopted when the load levels are high (stress and strain not linearly related). This type of behaviour has been commonly referred to as *low-cycle fatigue* or *strain-controlled fatigue*.

The most important problem related to Strain-Life approach is that deriving a strain-time history is more difficult than obtaining a stress-time history for the elastic case, and local stress-strain history must be determined (stress analysis procedures such as experimental strain measurements are usually required).

A fully understanding of the procedure needs a detailed description of how these local stresses and strains are found. Anyway the minimum needs for basic understanding may be summarized as:

- Strain is the basic cause of fatigue. At some point in the component being loaded the strain must be plastic for a crack to start.
- Plastic strain changes the properties of a material, especially the way it yields, when loaded later.
- When a local stress-strain history has been calculated, a valid cycle-counting method must be used to identify ranges of strain that are being applied.
- When strain cycles have been counted, experimental data from tests carried out under constant-strain conditions will be needed for the life estimation (not S-N data from conventional constant-load test).

The Strain-Life Curve

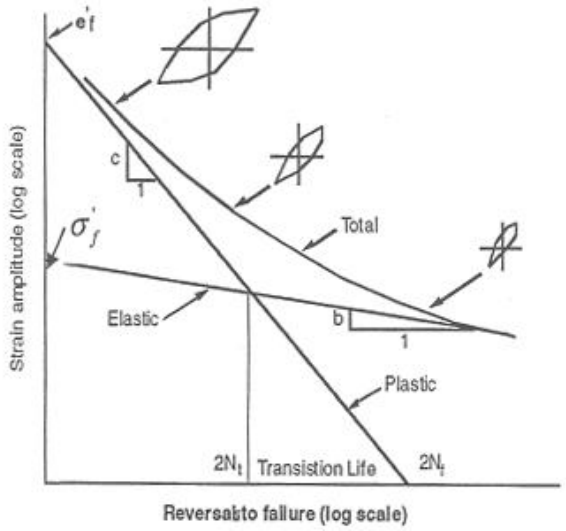

Fig 1.6

Coffin and Manson proposed a characterization of fatigue life based on plastic strain amplitude. They noted that when the logarithm of the plastic strain amplitude, $\Delta\varepsilon_p/2$, was plotted against the logarithm of the number of load reversals to failure, $2N_f$, a linear relationship resulted for metallic materials:

$$\frac{\Delta\varepsilon_p}{2} = \varepsilon'_f (2N_f)^c$$

where ε'_f is the fatigue ductility coefficient and c is the fatigue ductility exponent. In general, ε'_f is approximately equal to the true fracture ductility ε_f in monotonic tension.

Since the total strain amplitude in a constant strain amplitude test, $\Delta\varepsilon/2$, can be written as the sum of elastic strain amplitude, $\Delta\varepsilon_e/2$, and plastic strain amplitude, $\Delta\varepsilon_p/2$,

$$\frac{\Delta\varepsilon}{2} = \frac{\Delta\varepsilon_e}{2} + \frac{\Delta\varepsilon_p}{2}$$

the Coffin-Manson relationship provides a convenient engineering expression for characterizing the total fatigue life.

Noting that:

$$\frac{\Delta\varepsilon_e}{2} = \frac{\Delta\sigma}{2E} = \frac{\sigma_a}{E}$$

where E is the Young's modulus, it is found that:

$$\frac{\Delta\varepsilon_e}{2} = \frac{\sigma'_f}{E}(2N_f)^b$$

and at the end:

$$\frac{\Delta\varepsilon}{2} = \frac{\sigma'_f}{E}(2N_f)^b + \varepsilon'_f(2N_f)^c$$

The first and the second terms on the right hand side of this equation are the elastic and plastic components, respectively, of the total strain amplitude. This equation forms the basis for the strain-life approach to fatigue design.

The variations of the elastic, plastic and total strain amplitudes can be plotted as functions of the number of load reversals to failure, $2N_f$ (Strain-Life curve).

In order to examine the implications of Strain-Life curve for *short* and *long* fatigue lives, it is useful to consider a *transition life*, which is defined as the number of reversals to failure $(2N_f)_t$ at which elastic and plastic strain amplitudes are equal:

$$(2N_f)_t = \left(\frac{\varepsilon'_f E}{\sigma'_f}\right)^{1/(b-c)}$$

At short fatigue lives ($2N_f << (2N_f)_t$), plastic strain amplitude is dominant, so fatigue life of the material is controlled by ductility.

At long fatigue lives ($2N_f >> (2N_f)_t$), the elastic strain amplitude is more significant than the plastic one and the fatigue life is dictated by the rupture strength.

The Effect of Mean Stress

Mean stress effects have also to be incorporated into the uniaxial strain-based characterization of fatigue life. The *Morrow approach* proposes a modification for mean stress effects by modifying the baseline Strain-Life curve. The mean stress is taken in account by modifying the elastic part of the Strain-Life curve as follows:

$$\varepsilon_e = \frac{(\sigma'_f - \sigma_0)}{E}(2N_f)^b$$

where σ_0 is the mean stress.

The entire strain life curve then becomes:

$$\varepsilon = \frac{(\sigma'_f - \sigma_0)}{E}(2N_f)^b + \varepsilon'_f(2N_f)^c$$

The Morrow equation is consistent with the observation that mean stress effects are significant at low values of plastic strain and have little effect at high plastic strains.

1.2.3 Fatigue Crack Propagation Analysis

The Concept of Stress Intensity

Let's consider the stress field around the tip of the crack. This field can be expressed in such a way that all terms (normal and shear stresses) can have the common factor $\sigma(\pi a)^{1/2}$ extracted. Geometry, form of loading and the way the crack will extend also have effects that may be quantified for the

whole field. Combining these into a factor *Y*, we can identify a parameter that characterises the whole field near to the crack tip:

$$K = Y\sigma(\pi a)^{1/2}$$ crack tip stress intensity factor

If the crack extends when K reaches a critical value, we will have a criterion for determining the stress σ, which will extend a crack of a length a when Y has a certain value.

K critical value is a material property called fracture toughness (K_{Ic}).

Analysis is often limited to the case where the plastic zone near the crack tip is small (Linear Elastic Fracture Mechanism).

Fatigue Crack Propagation (FCP) and LEFM

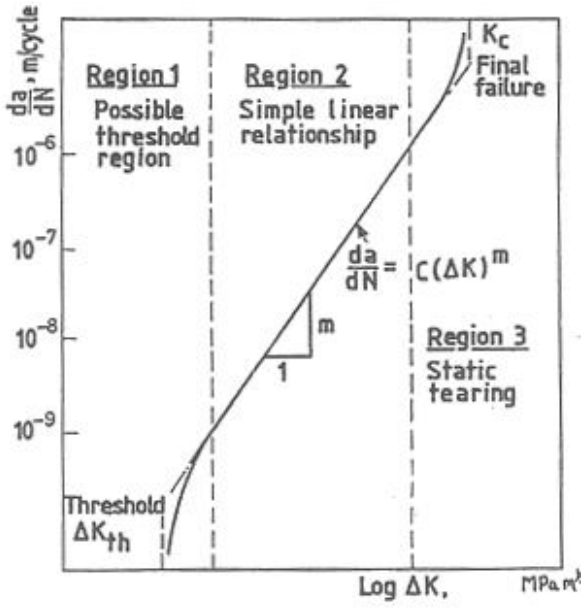

Fig. 1.7

If a crack is propagating under repeated loading, *a* will steadily increase and the value of *K*, when the dynamic load is at a maximum, will also increase. When this value K_{Max} reaches K_{Ic}, the crack will extend

catastrophically. In a constant amplitude fatigue test ranging from σ_{Max} to σ_{min}, values of K can be computed for the extremes of load (K_{Max}, K_{min}). The difference between these values is the range of crack tip intensity factor (ΔK). As the rate of crack propagation da/dN depends on ΔK, its value can be calculated. The rate will depend on σ and on crack length a, which will increase as the crack extends. To carry out tests at constant ΔK, crack length must be monitored and the range of load decreased in proportion to $a^{1/2}$.

The characteristic result of a FCP test is a curve reporting da/dN as a function of ΔK. Three regions are typically present.

The high crack-propagation rate at the beginning of the test is related to the sharpness of the notch tip created by razor blade. If the curve becomes vertical in this region, as it does in many reported data, there is a *threshold* value of ΔK below which the crack growth rate is zero.

For polymeric materials in the course of fatigue cycling the notch undergoes blunting (as a result of adiabatic heating during fatigue cycling and of the matrix viscoelastic behaviour) and the FCP rate decreases (deceleration) until a minimum value is reached. This lower value of the FCP rate has been associated to the development of a critical damage zone and/or critical damage density which corresponds to the onset of a stable FCP acceleration which is followed by crack instability and complete fracture. The most common expression used to describe the stable FCP acceleration zone is the *Paris-Erdogan equation*:

$$da/dN = C(\Delta K)^m$$

where da/dN = current rate of crack propagation

a = current crack length

C,m are material properties

Other equations were also proposed which account for other parameters such as the stress ratio R (Forman, Priddle, Walker, Schwalbe, Hall).

The curve obtained from the Paris-Erdogan equation is often called the *apparent* ΔK curve. In fact there are many effects that the Paris equation does not take into account, such as crack closure, corrosive environments, the influence of a notch and static fracture contributions. One way to model these effects is to derive an *effective* ΔK curve modifying the apparent ΔK curve through all three of its regions. This effective ΔK is then used in the Paris equation to determine crack growth.

1.3 Non Destructive Techniques

Since the Eighties, the research on the damage tolerance of polymer matrix composites has been focused on the assessment of damage within these materials. In order to monitor the damage development within these materials during static, fatigue and impact loading in possible different environmental conditions, several non-destructive techniques (NDT) are being applied.

Acoustic Emission Technique

It is a strictly passive NDT which listens to the elastic energy (ultrasound) being released when suddenly microstructural changes are taking place (crack development, delamination growth, fibre fracture, etc.). Different methods for signal processing are being developed to obtain a one-

to-one correlation with damage source and acoustic emission signal characteristics (peak amplitude, rise time, etc.) and frequency.

Microfocus Computer Tomography

It is a non-destructive inspection technique based on differences in absorption / attenuation of X-rays through the material. The CT-technique provides 2D-images of different sections of the sample. A high resolution 3D image may be reconstructed and defects / details in the order of 10 μm can be detected.

Stiffness Monitoring Techniques

These techniques periodically monitor material stiffness (for example using strain gauges) during exercise/fatigue testing. In case of anisotropic materials both longitudinal and transverse stiffness are monitored. The techniques allow detecting the onset of damage and the overall material response during long term experiments.

1.4 Fatigue of Polymer

It is well established that the fatigue response of polymeric materials has two distinct regimes.

At high frequencies and/or stress levels, the fatigue life of the polymer is dominated by hysteretic heating. This occurs as a consequence of the high internal damping and low thermal conductivity inherent in many polymers. Under these conditions, the polymer fails at relatively short

lifetimes. Hence, this regime is commonly referred to as the *thermally dominated* or *low-cycle regime*.

As the stress level and/or test frequency is reduced, another failure mode is observed. This failure mode is more brittle and the service life of the polymer is associated with the nucleation and growth of flaws in the material to a critical size. This regime is referred to as the *mechanically dominated* or *high-cycle regime*. Subcritical crack growth kinetics have been measured on a wide range of polymers and have generally shown to follow a Paris-type law once the flaw grows beyond the threshold flaw size. For many polymers, this threshold size is on the order of a 10^{-3} m [5]. When cracks are below the threshold size, their growth rates have been shown to not be well described by a Paris-type law (paragraph 1.2.1).

In practice two different mechanisms can prevail in fatigue: one in which crack initiation and growth prevails (well described by the Paris law) and another where a more general degradation takes place, without a crack being present. These differences are due especially to the stress level, the frequency and the matrix deformability, while also interface strength and filler orientation (if anisotropic) are important parameters.

The phenomenon of thermal softening is related to the dissipative nature of polymers[1], characterised by strong damping, which produces high mechanical hysteresis. This, together with their reduced thermal conductivity, can originate a significant temperature increase, especially at high loads and loading rates (figure 1.8). In these conditions thermal softening can become very relevant and overlap mechanical fatigue.

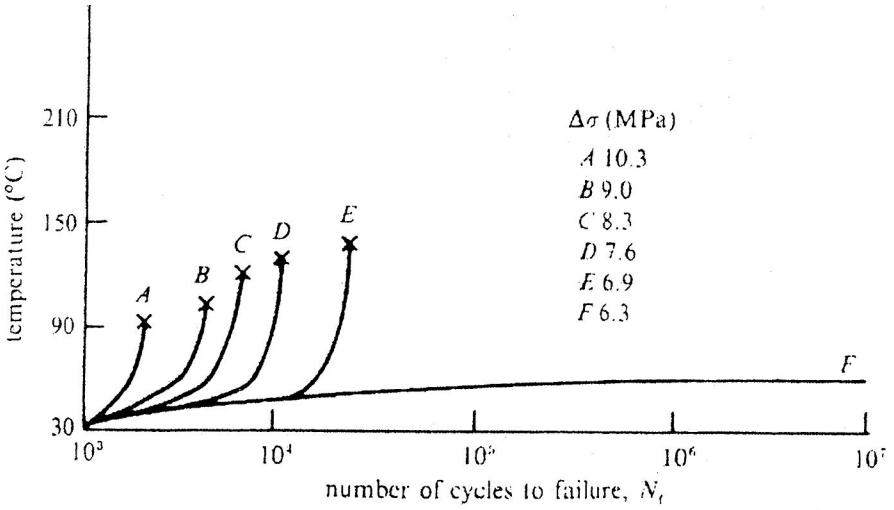

Fig 1.7: Effect of the applied stress range $\Delta\sigma$ on temperature rise in PTFE subjected to stress-controlled fatigue. The symbol "x" denotes failure of the specimen.

[1] The heat generated per unit of time and of material volume can be expressed by:

$$\dot{Q}_g = \pi f J \sigma_{\max}^2$$

f: frequency of the applied load, *J*: mechanical loss factor (associated to energy dissipated into heat); σ_{max} : maximum applied load. The actual increase of temperature (stable or instable) depends on the thermal exchange phenomena with the surrounding environment (related to specimen geometry and to the configuration of the experimental set-up).

[J.D. Ferry, *Viscoelastic Properties of Polymers*, 3rd ed., Wiley, New York, 1980]

Fatigue failure should not be thought only as the breaking of the specimen into two separate pieces, but as the progressive material damage accumulation resulting in a drastic reduction of mechanical properties (stiffness, strength) till reaching a completely useless condition for practical purposes. It is in fact well known that *cyclic softening* is the main fatigue phenomenon of ductile polymers [2]. Monitoring the material stiffness during the fatigue life enables the measurement of a damage rate.

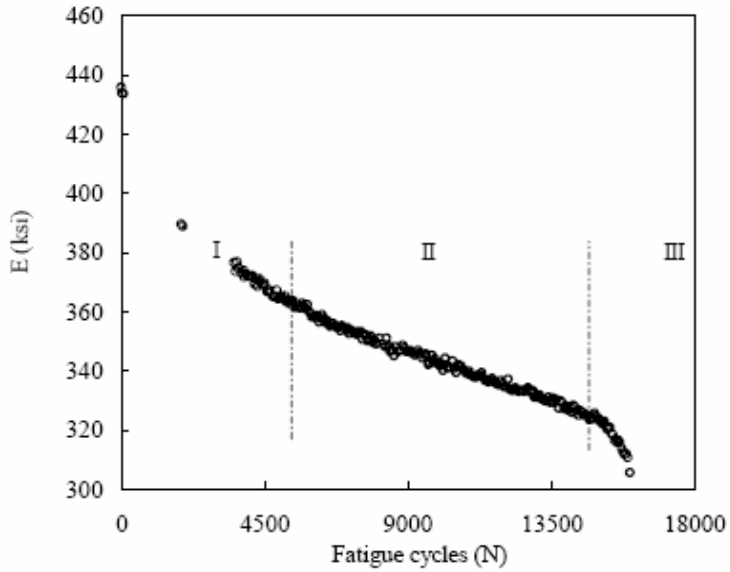

Fig 1.8: Stiffness reduction during flexural fatigue loading of a wood flour-filled HDPE [6]

The typical plot of the material stiffness during fatigue life is reported in figure 1.9 [6]. Three distinct regions can be identified. The first region shows a rapid decrease of coupon stiffness over the first few cycles: the extent of damage in this region correlates with the amount of damage observed in a quasi-static loading-unloading test to the same load. This then stabilizes in a linear region (second region) whose slope can be interpreted as a damage rate. This damage rate was shown to depend on the maximum

stress in the fatigue life [6]. Just prior to failure a rapid decrease in stiffness is again observed (third region) that may be associated with localization of damage in the failure zone.

The damage accumulation during fatigue loading manifests also as a progressive creep, resulting from the increasing material compliance produced by microstructural damage-evolution processes (crazing, shear-bands formation, cavitation, crack nucleation and propagation) and from internal heating produced by damping. This is particularly evident in S-N load-controlled fatigue tests where the elongations at the maximum and minimum loads tend progressively to shift towards higher values (figure 1.9).

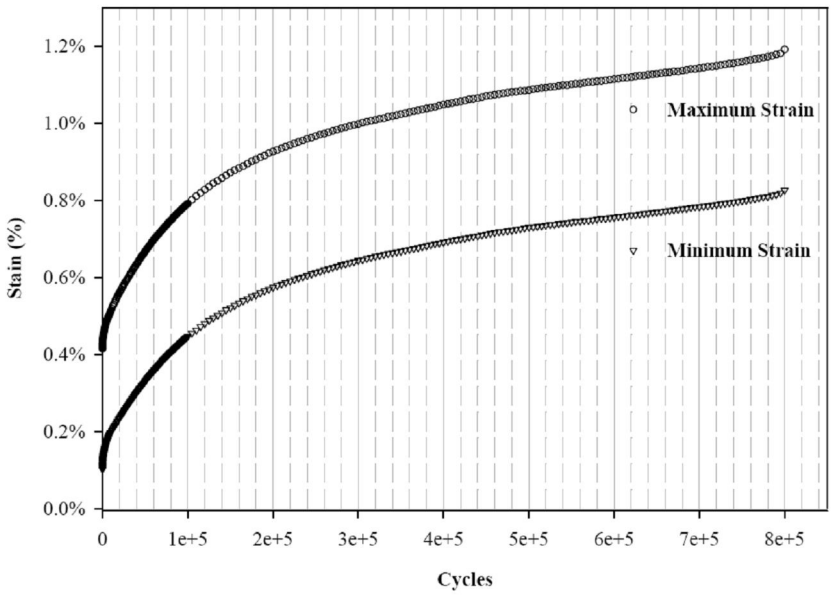

Fig 1.9: behaviour of a wood fibres-filled PP composite during a load-controlled S-N fatigue test [7]

It has been shown that the cyclic creep speed (the slope of the curves in figure 1.10 in the secondary stable region) presents a very good correlation with lifetime (number of cycles to failure) [8, 9]. The creep speed

can thus be used to predict the lifetime of a specimen while it is being fatigued.

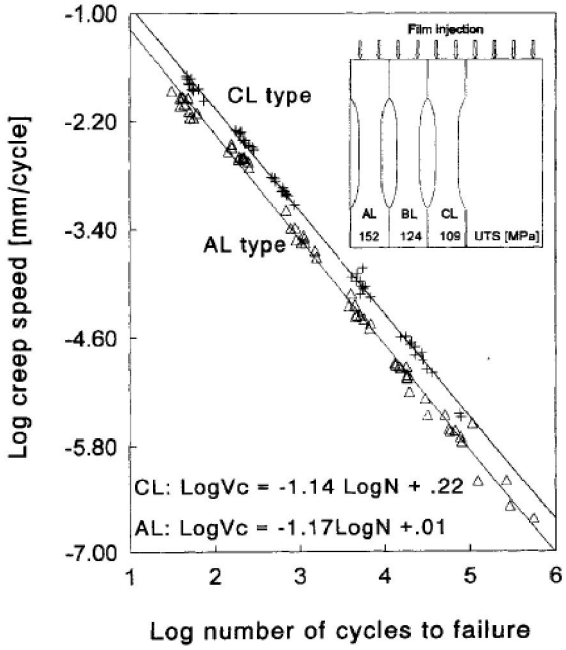

Fig 1.10: Creep speed vs. number of cycles to failure for various PA6-glass fibres formulations [8]

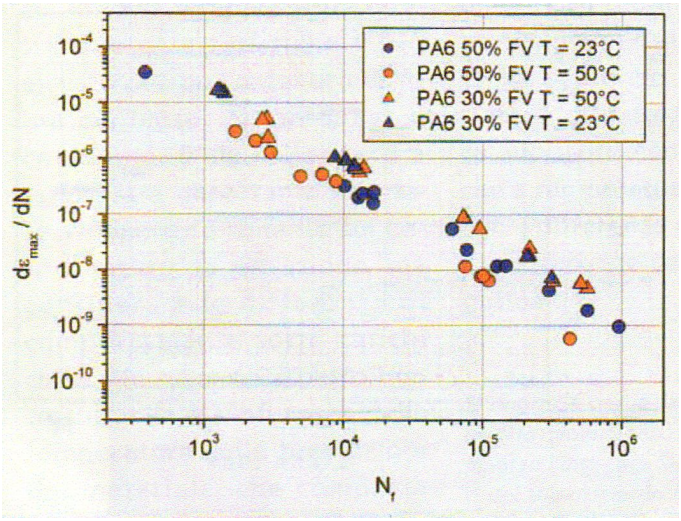

Fig 1.11: Creep speed vs. number of cycles to failure for various PA6-glass fibres formulations [9]

Under cyclic loading conditions the behaviour of polymeric systems is characterised by much higher creep rates than those observed in the case of static loading [10]. The experimentally observed phenomenon of accelerated time-dependent deformations of polymers subjected to cyclic loading regimes is defined as "vibro-creep."

There are two major factors that tend to determine the cyclic-creep rates and useful life of polymeric systems: *damage evolution* and *internal heating*. Damage-evolution processes in the presence of cyclic loads are different from that observed during quasi-static creep. The latter is characterised by continuously uniform microstructural changes in the material until the onset of tertiary creep (final instable creep phase), at which progressive damage localization tends to develop. In contrast, during cyclic creep, damage localization is initiated much earlier, almost at the very beginning of deformation immediately upon the loading application and tends to progress through several consecutive stages such as formation of crazes, craze growth, crack nucleation and crack propagation. These processes have an interactive effect through changes in the internal temperature which tends to further accelerate the cyclic creep.

Vibro-creep becomes stronger as the magnitude of the mean stress approaches the viscoelastic linearity limit. Creep rates tend to increase with increasing vibration amplitude, frequency and temperature.

A very important result underlined in several of the analysed works is that fatigue behaviour, especially at high stresses, is strongly related to the static strength of the material [4, 8, 11]. It was also supposed that the scatter in fatigue life is partially related to the variability in the fatigue strength of the tested specimens [4].

1.5 Fatigue-Induced Damage in PP

It has been reported that in isotactic PP fatigue damage evolves through craze formation and growth [5]. This is an important distinction compared to other polymers where fatigue damage evolves through micro-cracks formation: a craze contains load-bearing material (figure 1.13), while micro-cracks have no such load bearing material between the defect surfaces.

Fatigue loading (in the high-cycle regime) causes the initiation and propagation of crazes throughout the samples (typical craze dimensions are 1-100 μm). The crazes grow perpendicular to the stress direction. The energy required to form a craze was calculated to be of the order of 13 J/m^2 [5]. As the level of fatigue damage increases, craze–craze interaction becomes important and the crazes will coalesce. The increase in stress intensity in front of a craze will cause the initiation of many extra crazes, creating clusters of crazes. The damage density and the size of the crazes were observed to increase with the number of cycles (figure 1.13).

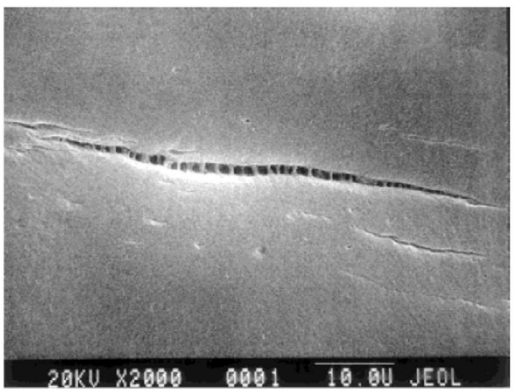

Fig 1.12: SEM image of a fatigued iPP sample showing detail of the crazed material between the faces of the craze [5]

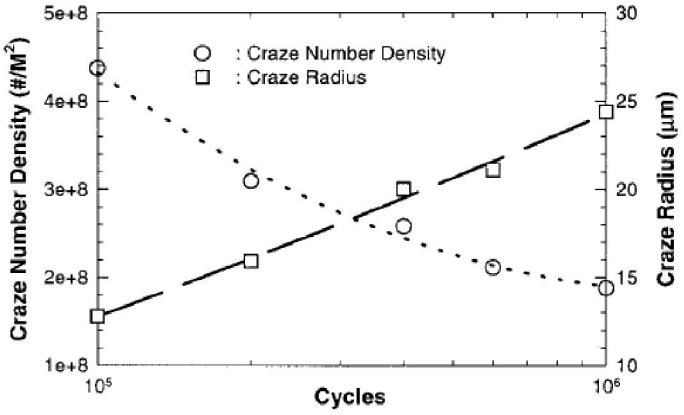

Fig 1.13: Evolution of craze damage during fatigue loading in PP [5]

Molecular weight and orientation of the skin-core morphology induced during the moulding process have been reported to influence the FCP performance of PP [12] (figure 1.15). In particular FCP rate tends to decrease with increasing molecular weight and with increasing orientation of the skin-core morphology in the direction of loading. A peculiar stable delayed crack growth range was observed just before the onset of the stable FCP acceleration. This is connected with the evolution of crazing and shear yielding processes resulting in crack tip blunting [12].

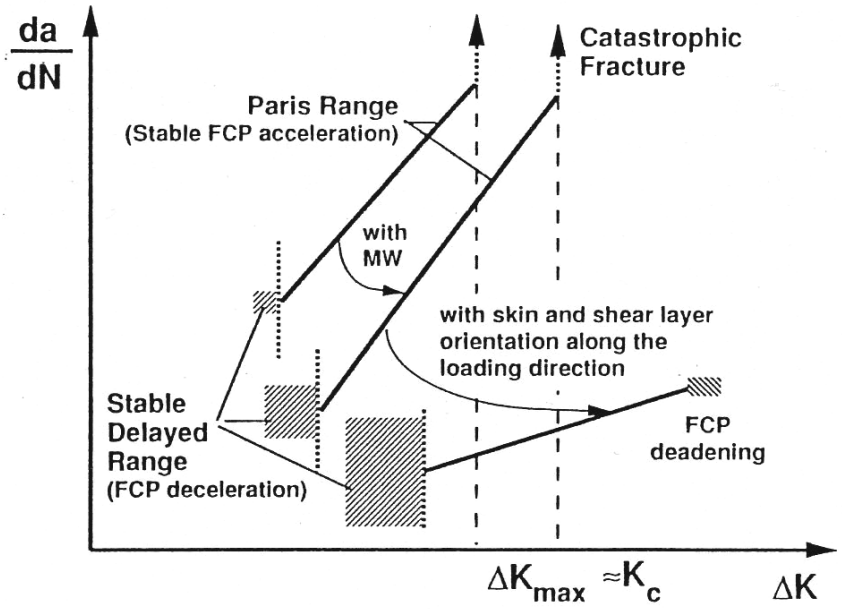

Fig 1.14: Effect of molecular mass (MW) and relative orientation of the skin-core structure on the FCP response of injection-molded PP [12]

1.6 Effect of Fillers on the Fatigue Performances of PP-Composites

1.6.1 Talc

As in the case of fibres and other anisotropic fillers, injection moulding causes a significant amount of anisotropy both in the static and fatigue properties of talc-filled PP systems. Both tensile and fatigue strengths of a 40 wt% talc-filled PP were in fact shown to be higher in the flow direction than those normal to the flow direction [13]. The orientation effect decreased at lower fatigue stress level. The presence of weld line reduced the fatigue strength. On the other hand, the fatigue strength showed very little

sensitivity to the presence of circular hole stress concentrators (with diameters from 1.6 to 6.35 mm).

1.6.2 Calcium Carbonate

A composite made of PP filled with calcium carbonate, mainly employed for household appliances' fabrication, was tested in fatigue under displacement control in simple bending [14]. The material did not undergo any fracture at macroscopic level, even when quite high deflection values were adopted. However a considerable loss in rigidity was measured, indicating that a modulus-based failure criterion could be appropriate in design. During the tests the material underwent evident plastic deformation without exhibiting a classical fracture in two pieces. Evident whitening propagated towards the upper surface and along the specimen length while the displacement was increased.

1.6.3 Wood Fibres

Coupled (with maleated PP) and uncoupled wood fibres/PP formulations were fatigued under load-controlled conditions at various frequencies [7]. Results indicated that cycles to failure increased with increasing frequency and the uncoupled formulations experienced greater temperature increases due to the longer fatigue life, when compared to the coupled formulations. The latter experienced a faster rate of internal heating when compared to the uncoupled as a result of the higher strength level imparted by the coupling agent producing a higher amount of mechanical energy available for converting to thermal energy.

Throughout all the fatigue tests, the specimens tended to fail at a constant strain (smaller than the strain at failure for the static tests).

1.6.4 Glass Fibres

The basic microscopic failure mechanisms occurring in discontinuous fibre-reinforced thermoplastics are shown schematically in figure 1.15 [12]. They can be grouped in *matrix-related* (crazing, voiding, fracture, shear yielding) and *fibre-related* (debonding, pull-out and fracture) mechanisms. For long glass fibre-reinforced thermoplastics, the latter are extended by fibre bridging, multiple fibre fracture and slippage of the fibres within a bundle.

Failure initiates first at the fibres ends. Stress concentration at the fibre ends within the damage zone gives rise to crazing in the PP matrix and debonding along the fibre is encouraged.

In cyclic fatigue of GF-PP there is always a change from semi-brittle (onset of FCP) to ductile-viscous type matrix failure (end of stable FCP range) due to the dissipated heat in the crack tip [12].

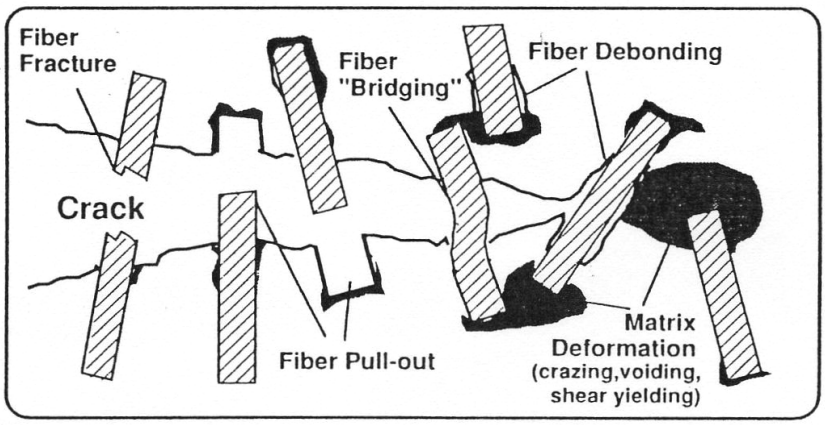

Fig 1.15: Failure mechanisms of discontinuous fiber-reinforced thermoplastics [12]

Gamstedt et al. [15] examined the fatigue mechanisms in PP and PP modified with maleic anhydride (MA-PP) reinforced by continuous longitudinal glass fibres. Shorter fatigue lives and more rapid reduction of the longitudinal Young's modulus of the glass-fibre/PP composite were observed and this was explained by its relatively poor fibre-matrix adhesion, which leads to wide-spread debond growth from fibre breaks and flaws. The growing debonds result in changing overloads in the surviving fibre segments, which in turn lead to further fibre breakage with ensuing debonding etc. (figure 1.16). Conversely, the glass-fibre/MA-PP demonstrates localized damage and non-propagating mechanisms, in which small matrix cracks form from flaws and are generally arrested by adjacent fibres. This results in a more fatigue resistant behaviour with longer fatigue lives (figure 1.17).

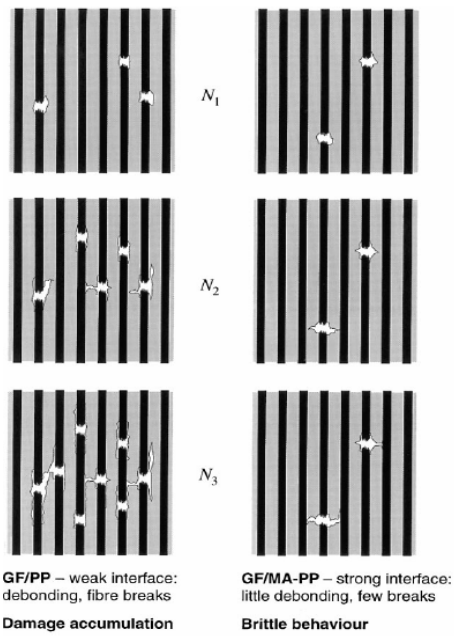

Fig 1.16: Schematic comparison of fatigue damage evolution in continuous glass-fibre/PP and continuous glass-fibre/MA-PP with increasing number of cycles ($N_1 < N_2 < N_3$) [15].

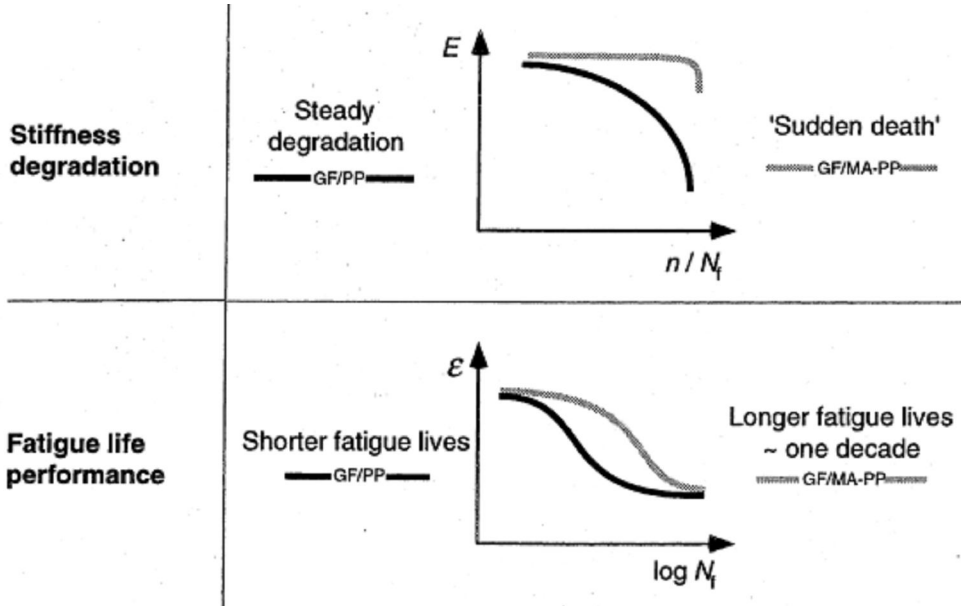

Fig 1.17: Comparison of fatigue performances in continuous glass-fibre/PP and continuous glass-fibre/MA-PP

It was reported that the presence of short glass fibres in isotactic PP reduces the tendency of this material to deform under fatigue and creep conditions and hence helps to prevent failure in load-bearing applications [16, 17]. In particular it was shown that an increase of the amount of glass fibres in a PP composite produced an improved resistance to fatigue crack propagation as a result of the reduced material compliance (figure 1.18).

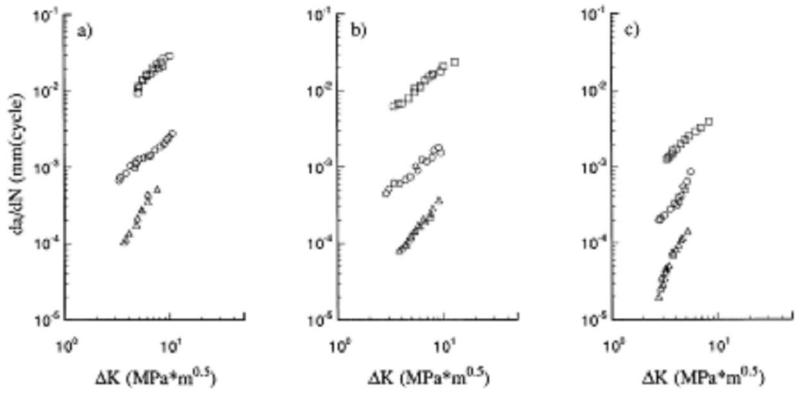

Fig 1.18: Paris plot (stable crack acceleration region) at 0.1 Hz (squares), 1 Hz (circles), 10 Hz (triangles) for composites reinforced with (a) 10 wt%, (b) 20 wt% and 30 wt% of short glass fibres (R = 0.4), from [16]

A study performed on short and long glass fibre-filled PP [12] showed that the resistance to FCP increases with increasing fibre volume fraction (v_f), with increasing amount of fibres aligned along the loading direction and with the l/d (length/diameter) ratio (figure 1.19).

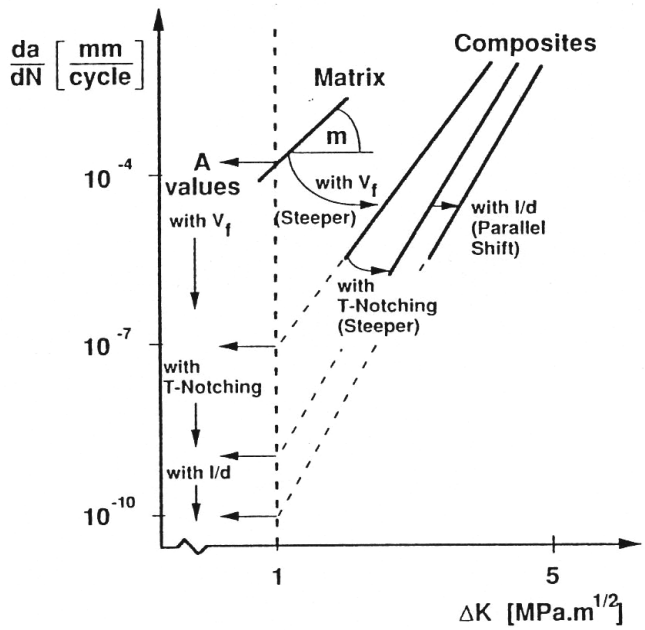

Fig 1.19: Glass fibres-filled PP FCP response as a function of microstructural parameters

As previously evidenced, when dealing with anisotropic fillers as fibres, a very important aspect that must be considered is the effect of fibre orientation on the material properties. A. Bernasconi et al. [18] evidenced how the fatigue strength varies with respect to the angle between fibres (supposed uniaxial) and the loading direction in tension uniaxial tests (figure 1.20).

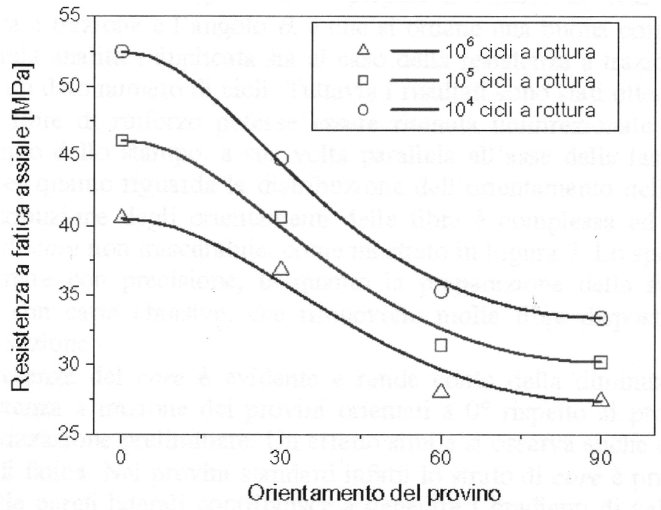

Fig 1.20: Fatigue strength for a given number of life cycles as a function of the angle between fibres (supposed uniaxial) and the loading direction in tension uniaxial tests [18]

The same authors gave indications about the role of recycling on the fatigue performances of glass-fibres filled PA. Ri-extrusion caused a sensible decrease of the average length of the fibres, resulting in reduced both static tensile strength and fatigue strength.

1.6.5 Nano-Clays

The fatigue performances of PP has been reported to be improved by the presence of small concentrations of organically modified clays (nano-clays) [19, 20]. In both works found on PP nanocomposites the fatigue failure

of specimens during S-N tests appeared to be initiated at large particles constituted by the agglomeration of several nanoparticles.

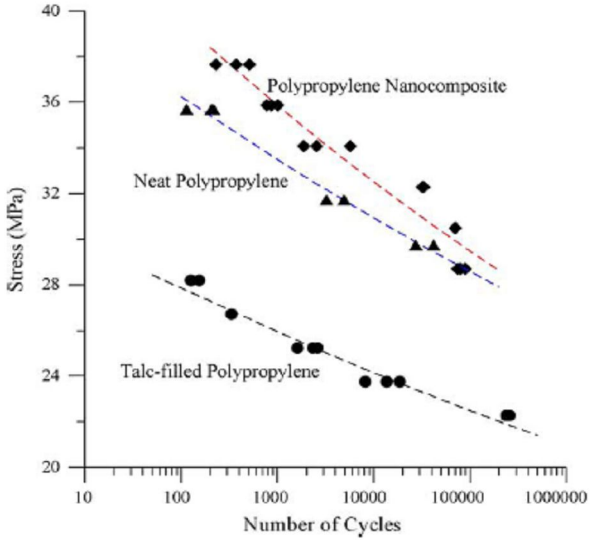

Fig 1.21: Fatigue S-N curves of polypropylene and its composites. Compositions: 5 wt% nano-clay, 40 wt% talc [19]

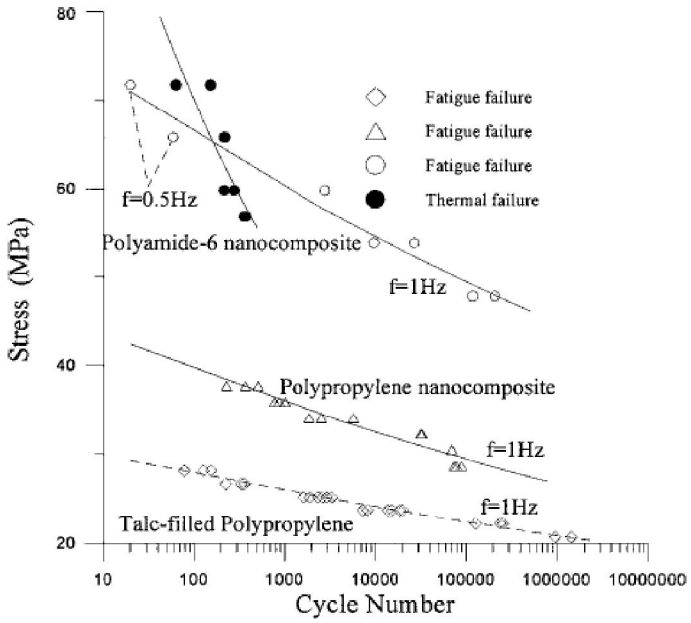

Fig 1.22: Fatigue S-N curves of PP (5 wt% nano-clay) and PA6 (3 wt% nano-clay) nanocomposites compared with a 40 wt% talc-filled PP [20]

1.7 Effect of Moulding Conditions on Fatigue Performances

Only one paper was found on the effects of moulding conditions on PP-based composites [21]. In particular it examined the effects of melt temperature and hold pressure on the static tensile and fatigue behaviour of an injection moulded 40 wt% talc-filled PP (anisotropic material).

For specimens in the flow direction, both yield strength and fatigue strength increased with increasing hold pressure, but they were relatively insensitive to melt temperature. For specimens normal to the flow direction, both yield strength and fatigue strength increased with increasing hold pressure and decreased with increasing melt temperature. For specimens containing a weld line, the yield strength and fatigue strength increased, with increasing hold pressure as well as increasing melt temperature. The observed differences in properties were explained in terms of the different skin-core morphology induced by the different processing conditions, and in particular to the different degree of talc particles orientation in the core and in the skin. In general, the greater the particle orientation parallel to the loading direction, the higher is strength, since they are more effective in stress transfer than those oriented normal to the loading direction.

In the Basquin equation (paragraph 1.2.1) fitting the experimental S-N curves, processing conditions influenced more the fatigue strength coefficient (σ_f) than the exponent b.

1.8 Effect of Testing Conditions

1.8.1 Loading Wave-Form

Waveforms with a non-zero mean stress value result in simultaneous creep and fatigue loading.

The most common waveform in fatigue testing is the sinusoidal. A square wave, for each frequency, leads to a reduction of the load level for which thermal softening occurs and this is due to the higher amount of energy dissipated per cycle. Moreover square waveforms produce clear creep response in concert with fatigue. For a triangular loading wave the situation is exactly the opposite.

Propagation rate for amorphous polymers decreases in the order: square > sinusoidal > triangular waveform.

1.8.2 Mean Stress

The total fatigue life derived from constant stress-amplitude fatigue tests decreases with increasing mean stress [2].

1.8.3 Type of Control

In load control, during fatigue testing, a temperature increase produces higher deformation, this results in higher energy dissipation, producing in its turn a further temperature increase. Thus an interactive process starts which can lead to failure for thermal softening in short time if the heat transferred to the environment is too low. In strain deformation instead a temperature increase produces stiffness reduction, resulting in this

case in reduced stress amplitude. There is then a reduction of energy dissipation and a consequent temperature reduction resulting in a self-stabilizing mechanism and a failure for thermal softening is much less probable.

1.8.4 Type of Load

In general a material has higher fatigue strength when subjected to cyclic bending tests than when subjected to cyclic uniaxial load. This is due to the existence of a stress gradient inside the sample cyclically bent. Fatigue cracks form easily and quickly on the surface for the high stresses present here, but the following propagation phase will be shorter for the lower stress levels inside the sample. The presence of a stress gradient will also delay failure for thermal softening.

1.8.5 Frequency

Increasing test frequency typically results in a reduction of fatigue life [2].

In general cyclic frequency determines the failure mode of polymers during fatigue tests, which can be either a thermal failure or a fatigue failure. However the sensitivity to frequency depends on the polymer type. For example PMMA and polyoxymethylene show strong sensitivity to frequency, while PA 6.6 and PC show little or no sensitivity to frequency. Frequency also determines the stress level at which thermal failure occurs before fatigue failure.

The effect of the test frequency on a PP-based system was studied for a 40 wt% talc-filled PP [13]. S-N tests were carried out in load control with a stress ratio R of 0.1 at various frequencies. The effect of cyclic frequency on the fatigue life is reported in figure 24. When the frequency was less than or equal to 2 Hz, the failure mode was due to fatigue and the fatigue life increased with frequency. However when the test frequency was greater than or equal to 5 Hz, the failure of the talc-filled PP was due to thermal softening and the fatigue life did not appear to be influenced much by the frequency.

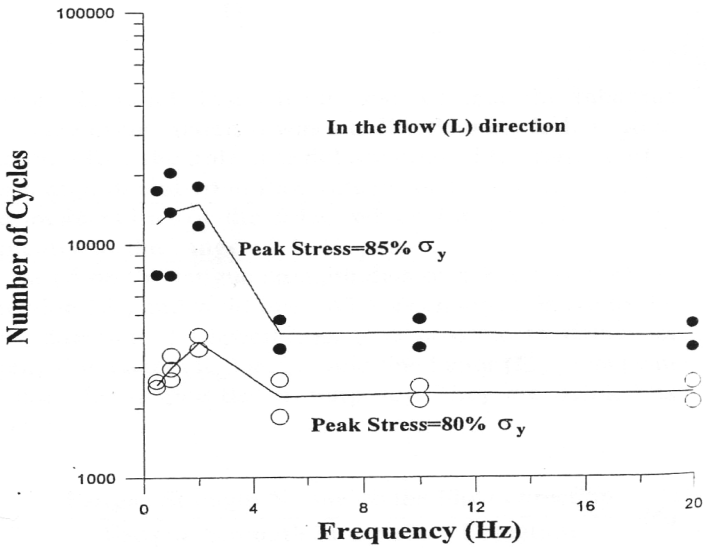

Fig 1.23: Effect of cyclic frequency on the fatigue life of 40 wt% talc-filled polypropylene [13]

1.8.6 Stress Ratio

It has been reported that for a given maximum stress the fatigue life notably increases with increasing R [4]. It was also reported that the scatter in fatigue life at high stresses tends to increase with increasing stress ratio [4].

References

[1] N. W. M. Bishop, F. Sherratt, *Finite Element Based Fatigue Calculations*, NAFEMS Ltd, 2000

[2] *Fatigue of Materials*, 2nd ed., S. Suresh, Cambridge Univ. Press. (1998)

[3] Y.L. Lee, J. Pan, R. Hathaway, M. Barkey, *Fatigue Testing and Anslysis – Theory and Practise*, Elsevier, 2005

[4] Flexural Fatigue Bahaviour of Random Continuous-Fibre-Reinforced Thermoplastic Composites", G. Caprino, A. D'Amore, *Composites Science and Technology*, 58, 957-965 (1998)

[5] Morphological Study of Fatigue-Induced Damage in Isotactic Polypropylene, A.J. Jones, A.J. Lesser, *Journal of Polymer Science Part B: Polymer Physics*, vol. 36, 2751-2760 (1998)

[6] *Durability Assessment and Modelling of Wood-Thermoplastic Composites*, S. Rangaray, Master Thesis (1999), Washington State University

[7] *Design and Fatigue of a Structural Wood-Plastic Composite*, A.E. Slaughter, Master Thesis (2004), Washington State University

[8] Mechanisms of Fatigue in Short Glass Fibre Reinforced Polyamide 6, J.J. Horst, J.L. Spoormaker, *Polymer Engineering and Science,* vol. 36, no. 22, 1996

[9] A. Bernasconi, P. Davoli, A. Basile, S. Gatti, Progettare con le Poliammidi: la Resistenza a Fatica della PA6 Rinforzata con Fibre di Vetro, InterPlastics, October 2003, pp. 78-85

[10] Cyclic Creep of Polymers and Polymer-Matrix Composites, A.M. Vinogradov, S. Schumacher, *Mechanics of Composite Materials*, vol. 37, no. 1, 29-34 (2001)

[11] Fatigue Behaviour of PMMA/Si Acrylic Casting Dispersions, J.D. Costa, J.M. Ferreira, C. Capela, *Materials Science and Technology*, 17, 1657-1663 (2001)

[12] J. Karger-Kocsis, Polypropylene - Structure, Blends and Composites. Volume 3 Composites, Chapman & Hall, 1995

[13] Fatigue Performance of an Injection Molded Talc-Filled Polypropylene, Y. Zhou, P.K. Mallick, *Polymer Engineering and Science*, vol. 45, no. 4, April 2005, pp. 510-516

[14] Young's Modulus Degradation in Fatigue of Filled Polymers for Household Appliances, Leone C.; Caprino G., *Plastics, Rubber and Composites*, Volume 32, Numbers 8-9, October 2003, pp. 345-348(4)

[15] Fatigue mechanisms in Unidirectional Glass-fibre-reinforced Polypropylene, E. Kristofer Gamstedta, Lars A. Berglund, Ton Peijs, *Composites Science and Technology,* 59 (1999) 759-768

[16] Fatigue Crack propagation in Polypropylene Reinforced with Short Glass Fibres, A. Pegoretti, T. Riccò, *Composites Science and Technology*, 59, 1055-1062 (1999)

[17] Growth in Discontinuous Glass Fibre Reinforced Polypropylene under Dynamic and Static Loading Conditions, A. Pegoretti, T. Riccò, *Composites: Part A*, 33 (2002) 1539–1547

[18] A Bernasconi, P. Davoli, A. Basile, A. Filippi, Effetto dell'Orientamento delle Fibre sulla Resistenza a Fatica di una Poliammide Rinforzata con Fibre di Vetro, Associazione Italiana per l'Analisi delle Sollecitazioni, XXXIV Convegno Nazionale, 14-17 Sept 2005, Politecnico di Milano

[19] Experimental Study on Thermal and Mechanical Behavior of Polypropylene, Talc/Plypropylene and Poypropylene/Clay Nanocomposites, Yuanxin Zhoua, Vijay Rangari, Hassan Mahfuza, Shaik Jeelani, P.K. Mallick, *Materials Science and Engineering A*, 402 (2005) 109–117

[20] Yield and fatigue behavior of polypropylene and polyamide-6 nanocomposites, K. Mallick and Yuanxin Zhou, *Journal of Materials Science*, Issue: Volume 38, Number 15 , Date: August 2003, Pages: 3183 -3190

[21] Effects of melt temperature and hold pressure on the tensile and fatigue properties of an injection moulded talc-filled polypropylene, Yuanxin Zhou, P.K. Mallick , *Polymer Engineering and Science*, Volume 45, Issue 6 , Pages 755 – 763, 2005

2

Accelerated fatigue test

Standard fatigue test requires long time to test a single material. The aim of this study is to develop a faster procedure to differentiate materials damage accumulation with a reduced number of cycles in shorter times than those required by conventional life tests.

The Accelerated Fatigue Test (AFT) developed is a new fast method to get information about material damage with the application of a tensile oligocyclic load with different max load levels (in terms of % tensile yield stress) by using a standard universal testing machine. In order to calculate the characteristic parameters for comparing the different materials, a dedicated Matlab® program has been developed. In particular we chose as indicators of the cumulative damage for the tested sample the area of the stress-strain cycle, the evolution of the elastic modulus and the residual strain trend [1, 2, 3].

The accelerated fatigue test was applied to different PP composites in order to understand their fatigue properties and the induced cumulative

damage and then compared with data obtained from conventional fatigue test in order to validate the new method.

2.1 Test conditions

The samples (injection moulded ASTM standard “dog-bone”) have been tested by uniaxial tensile tests conducted at room temperature in an Instron *5583 universal testing machine*.

The AFT is based on a constant amplitude stress level applied at a constant rate. The loading conditions have a triangular waveform. As the testing machine used only allowed to control the crosshead speed and to set the maximum and minimum stress level, the frequency cannot be maintained constant during the test. The maximum stress level is selected on the basis of the tensile properties (yield or maximum stress) of each material tested, while the minimum stress level is zero. Each test consists of a maximum of 6000 cycles. The crosshead speed is selected as the maximum allowed by the measurement device (50 mm/min). The strain is measured by the Instron video-extensometer, while the stress is calculated by the Instron software Merlin by dividing the load for the sample area. The data are captured with a frequency of 10 Hz and digitally stored for each cycle throughout the duration of the test.

As it is possible to notice, there are relevant differences between AFT and conventional fatigue test. Usually a conventional fatigue test on plastic materials is run at frequencies within 3 and 5 Hz [4, 5, 7]. As a consequence the loading conditions have a sinusoidal waveform and it is possible to test a

sample at different load level, even at low maximum stresses, in order to build the Wöhler diagram. The limits of this kind of method are given by the long time required to get the results and by the need of a device *ad hoc* for the test. The most important goal scored by AFT is the overcoming of these restrictions. In fact our method does not require a specific dynamic device and is able to evaluate two loading conditions per day. Obviously there is a price to pay to reach these results. The major restrictions of AFT are represented by the fact that using a static device, it is impossible to control the loading frequency and to maintain its value constant during the test. Moreover the maximum crosshead speed allowed by the instrument used, leads to run the test at frequency values three order of magnitude lower than those set up in a conventional test. For these reasons it is impossible to get information as complete as those from a fatigue test. In particular by following AFT method the Wöhler curve cannot be built, because usually the sample does not reach breaking conditions. This means that generally from AFT the information acquired regards a trend toward breaking conditions. As a consequence, the higher is the maximum stress set up, the more a trend is emphasized.

Summing up the considerations about the setting of AFT, it is possible to say that the method gives information about the tendency of a sample to reach damaging conditions in really little time.

2.2 Test data elaboration

The first problem encountered to describe the fatigue behaviour of the tested materials was to identify which parameters to use to follow the progressive material damage.

G. Tao and Z. Xi [6], for example, studied the uniaxial fatigue behaviour of an epoxy resin with non-contact real-time strain measurement and control system. A relation of strain amplitude vs. fatigue life for fully-reversed strainrange-controlled uniaxial fatigue tests was obtained. Quantitative analyses of evolutions of various mechanical properties (including stress range, elastic modulus, nonlinear stress-strain relation, dissipated strain energy density, etc.) during the entire fatigue life period were carried out based on recorded stress-strain data. From the evolution of the stress-strain hysteresis loops, a gradual degradation of modulus and a decrease of nonlinear effect in stress-strain response were observed. The authors also found that these two phenomena were independent of the loading control mode (stress-control or strain-range-control) and of the mean stress/strain values in the cyclic loading.

A similar approach was applied in this work for the evaluation of the AFT data. A progressive modification of the shape of the hysteresis loops could be observed during the fatigue test, resulting from the progressive changes of various material mechanical properties (progressive damage accumulation). In particular for each cycle the following parameters were considered [1, 2, 3]:

- *Secant Modulus, E [MPa];*
- *Relative Secant Modulus, E_i/E_0;*

- *Hysteresis Loop Area [J 10^{-3}];*
- *Dissipated Strain Energy [J/cm^3];*
- *Maximum Strain, ε_{max} [%];*
- *Minimum Strain or Residual Deformation, ε_{min} [%];*
- *Strain Range, $\Delta\varepsilon$ [%];*

Supposing that only the gauge length of the injected molded ASTM standard "dog-bone" shaped tests specimen participates to sample deformation, the stress was calculated as:

Stress [MPa] = Crosshead Load [N]/ Gauge section of specimen [mm^2]

while, as mentioned above, the strain was evaluated by the Instron video-extensometer.

The secant modulus E, was computed from the stress-strain curve as the slope of hysteresis loop (Figure 2.1).

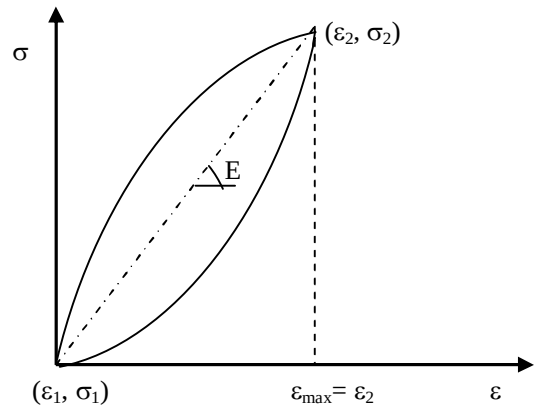

Fig. 2.1: secant modulus

To calculate this slope we considered in the stress-strain plot the first point (ε_1, σ_1) of the hysteresis loop and the point that corresponds to the maximum longitudinal strain (ε_2, σ_2) for each cycle.

$$E = \frac{\sigma_2 - \sigma_1}{\varepsilon_2 - \varepsilon_1} \cdot 100$$

The drop of the secant modulus is the ratio of the secant modulus of the first cycle (at which the material is supposed not damaged), E_0, and its value at the i-th cycle, E_i.

The hysteresis loop area (dissipated strain energy) was calculated by integrating, with the trapezoidal integration method, the stress versus strain plot for each cycle.

The difference between the maximum and minimum strain gives the strain range, $\Delta\varepsilon$.

$$\Delta\varepsilon = \varepsilon_{MAX} - \varepsilon_{MIN}$$

From the comparison of these parameters we could emphasize the differences in the fatigue behaviour of the different materials examined.

2.3 Materials and materials properties

Different groups of materials were considered, in order to verify the usefulness of AFT method in testing a wide range of composites. All the materials tested are Polypropylene based, but reinforced or with different kind of filler, or prepared in different formulations and/or based on different PP matrices. The PP matrices used in the materials are general purpose isotactic homopolymer suited for both technical and packaging injection moulded components. The fillers used are all commercial products from different suppliers.

First of all we have considered three different $CaCO_3$-PP microcomposites were prepared by varying the PP matrix (EC1, EC2, EC3). All the samples contain about 40 wt% of micrometric ground calcium

carbonate and others additives (mainly antioxidants). The aim of this first test was to prove that AFT is effective in testing materials with the same formulation but based on matrices provided by different suppliers. In table 1 mechanical propertied of the three materials are reported.

	EC1	EC2	EC3
PP MFI [g/10min] - matrix	7	7	5
% filler	40	40	40
Tensile yield stress [MPa]	22	23	24
Tensile yield strain [%]	3.4	4.0	3.0
Tensile stress at break [MPa]	17	16.8	18.3
Tensile strain at break [%]	60	60	65
Flexural Modulus [MPa]	3200	3200	3400
80% of yield stress [MPa]	17,5	18,2	19,5

Tab. 2.1: EC group mechanical properties

The second group examined is constituted by $CaCO_3$-Glass-fibre-PP composites (ECH1, ECH2), mainly made by 21 wt % of $CaCO_3$ (added with the PP matrix), 15 wt% of glass fibres and 0.5 wt % of others additives. In this case the difference between the samples is given by the preparation steps. In fact for ECH1 the matrix, the fillers and the additives have been pre-mixed in a dry blender and then extrusion compounded, before that tensile and flexural test samples, according to ASTM D 638 and to ASTM D 790, have been injection moulded from the pelletised extrudate. On the contrary, ECH2 samples have been injection moulded directly after the dry blended phase. In order to prevent problems of good dispersion of the GF, a different matrix, more reach in additives, have been used. In tab. 2 their mechanical properties are reported.

	ECH1	ECH2
Tensile yield stress [MPa]	-	-
Tensile yield strain [%]	-	-
Tensile stress at break [MPa]	51.5	74
Tensile strain at break [%]	3	2.4
Flexural Modulus [MPa]	4200	4700

Tab. 2.2: ECH group mechanical properties

In the third set have been compared the properties of $CaCO_3$-PP composites (EX1, EX2) added with two different blowing agents. These kinds of materials have been formulated with the double purposes of cost and weight reduction on components production, thanks to a lesser presence of PP in the formulation. In the following table the tensile ad flexural properties are compared.

	EX1	EX2
Tensile yield stress [MPa]	18.5	18.8
Tensile yield strain [%]	3.0	3.3
Tensile stress at break [MPa]	15.8	16.6
Tensile strain at break [%]	28.8	23.8
Flexural Modulus [MPa]	3350	3384
80% of yield stress [MPa]	14.8	15.0

Tab. 2.3: EX group mechanical properties

After the comparison between materials of the same group, in the next chapter we will try to compare materials coming from different group, meaning of completely different mechanical properties and fatigue behaviour. These comparisons will emphasize the role of the parameters we have chosen in describing fatigue behaviour.

References

[1] Morphological Study of Fatigue-Induced Damage in Isotactic Polypropylene, A.J. Jones, A.J. Lesser, *Journal of Polymer Science. Part B: Polymer Physics*, vol. 36, 2751-2760 (1998)

[2] *Durability Assessment and Modelling of Wood-Thermoplastic Composites*, S. Rangaray, Master Thesis (1999), Washington State University

[3] *Design and Fatigue of a Structural Wood-Plastic Composite*, A.E. Slaughter, Master Thesis (2004), Washington State University

[4] Y.L. Lee, J. Pan, R. Hathaway, M. Barkey, *Fatigue Testing and Anslysis – Theory and Practise*, Elsevier, 2005

[5] *Effects of time and temperature conditions on the tensile-tensile fatigue behaviour of short fiber reinforced polyamides,* N. Jia, V.A. Kagan, *Procs of ANTEC'97,* 1997

[6] G. Tao, Z. Xia, *Polymer Engineering and Science*, 47, 780-788 (2007)

[7] Fatigue Performance of an Injection Molded Talc-Filled Polypropylene, Y. Zhou, P.M. Mallick, *Polymer Engineering and Science,* 45, 510-516 (2005)

3

Results and discussion

As we have anticipated in the previous chapter, the applications of AFT method have been divided into different steps. In the first part three groups of materials, quite similar for composition and mechanical properties, have been compared with the purpose of demonstrate the utility of the AFT for industrial applications. In fact in these cases a fast method able to compare, for example, the fatigue behaviour of two or more matrices furnished by different suppliers or the consequence of a little variation in the formulation of a composite prepared with the aim of cost reduction, could be fundamental.

In the second part of the chapter, AFT was applied to different PP-based composites, in order to understand their fatigue properties and as the composition and the different kind of fillers influence the trend of the damage parameters.

3.1 EC materials group

As illustrated previously, these materials differ only for the PP matrix used in the formulation. All of them were tested at the 80% of their yield strength. In the following figure the trend of the elastic modulus or, more precisely, of the relative modulus (E_i/E_0), is represented.

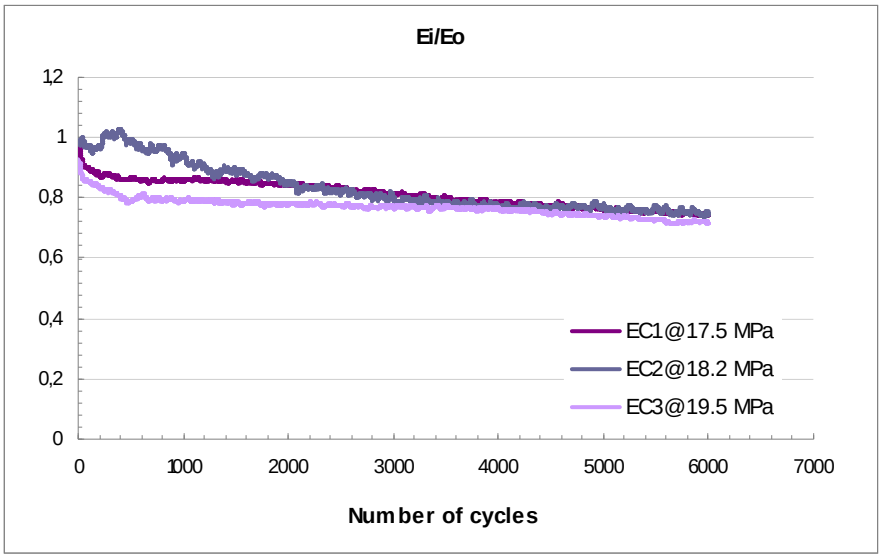

Fig. 3.2: EC group relative moduli trends

What is important to observe is the rate of decay for the three moduli. Calculating the trend line with the help of Microsoft Excel, what emerges is that the decay trend is well represented by a power law for all the samples ($y = A*x^B$), and that the rate of decay is faster for material EC2. In table 1 that results are reported.

	A	B	R^2
EC1	1.16	0.05	0.76
EC2	1.56	0.082	0.83
EC3	1.01	0.035	0.86

Tab. 3.4: power law parameters and R^2 values for EC materials

Before comparing the other parameters it is important to point out that both the stress and strain scales of the stress-strain curves have been multiplied for a factor A that is:

A = 80 / max stress value considered

In this way it was possible to compare materials tested at different stress value (but however at the 80% of their yield or maximum stress) on the same scale.

In fig. 3.2 the area trend for each material is represented.

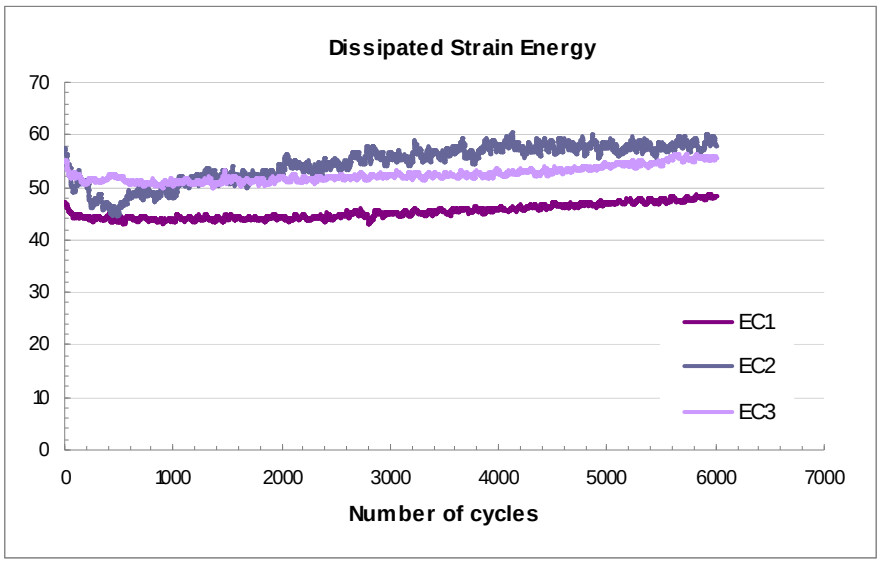

Fig. 3.3: cycles' area trend for EC group

The results substantially confirm that EC2 has a major tendency to dissipate energy when undergoes fatigue, meaning a lesser resistance. About EC1 and EC3, they show a quite similar behaviour. Although EC3 has higher area values, the rate of increase is slightly slower, as is demonstrated by the equation of the Microsoft Excel trend line. In this case the curves are quite

well fitted by an exponential equation ($y = A*e^{(B*x)}$) whose parameters are reported in table 3.2.

	A	B	R^2
EC1	43.25	2E-05	0.81
EC2	49.13	3E-05	0.77
EC3	50.42	1E-05	0.73

Tab. 3.5: exponential equation parameters describing cycles' area trend

In conclusion, materials EC1 and EC3 show quite similar fatigue properties, but it is important to remember that EC1 has higher mechanical characteristics, and that if tested at the same maximum stress level, EC3 would demonstrate longer life endurance.

This fact has been proved and the result is plotted in the next figure

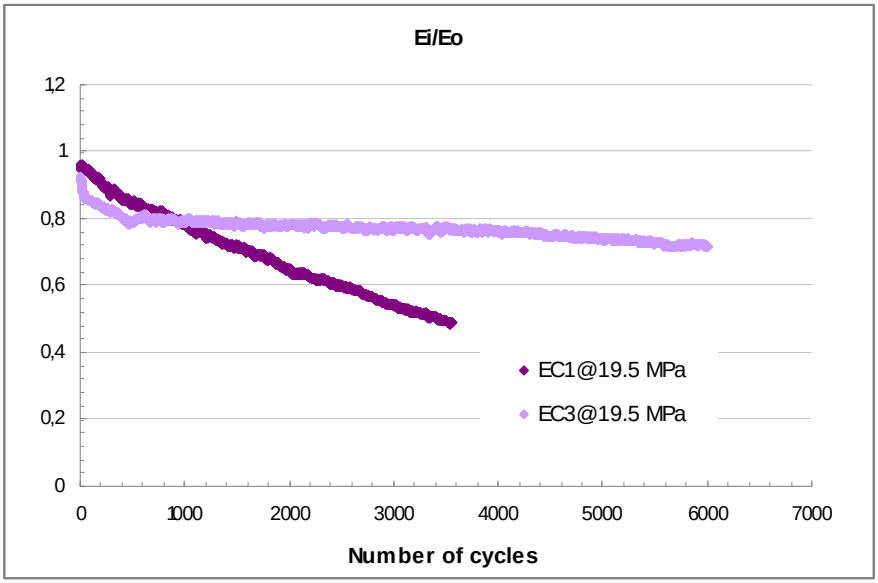

Fig. 3.4: comparison between EC1 and EC3 relative moduli at 19.5 MPa

In these conditions EC1 shows a dramatic decay of the secant modulus towards breaking conditions.

3.2 ECH materials group

The main difference between the ECH1 and ECH2 is given by the length of the glass fibres in the formulation. In fact, as a consequence of the two preparation paths followed and depicted in the previous chapter, in the former material the glass fibres are considerably shorter that in the latter. Since the effect of the glass fibres length is clear in term of mechanical properties, let's see what it means from a fatigue point of view. In the following graph a comparison between the relative modulus is illustrated.

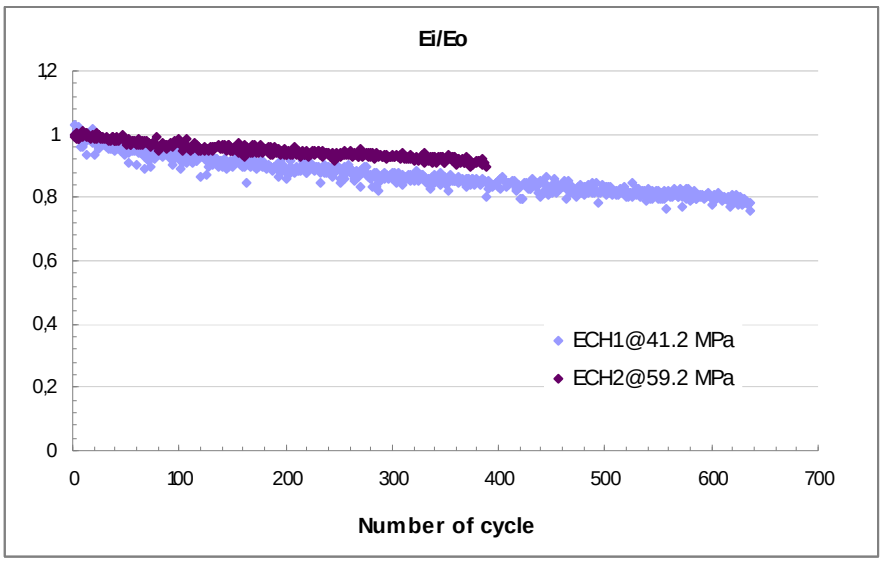

Fig. 3.5: ECH1 Vs ECH2 relative modulus trend

As expected, ECH2 shows a slower rate of decay, but on the other hand, reaches breaking conditions after fewer cycles. This fact could be due to the higher rigidity of ECH2, although it is hazardous to generalize this consideration, even if, after several tests, this tendency has been substantially confirmed, but both the materials break at a number of cycles of the same order of magnitude. In my opinion it is more considerable to focus our attention on the trend of the modulus. It is important to underline

that for materials that reach breaking or yielding conditions, the modulus trend is described by exponential equation better that by a power law. In table 3.3 the parameters of the exponential law are reported.

	A	B	R^2
ECH1	0.96	-3*E-04	0.91
ECH3	50.42	-2*E-04	0.88

Tab. 3.6: exponential law parameters describing the modulus decay for ECH1 and ECH2

The trend of the area values emphasizes the difference between ECH1 and ECH2.

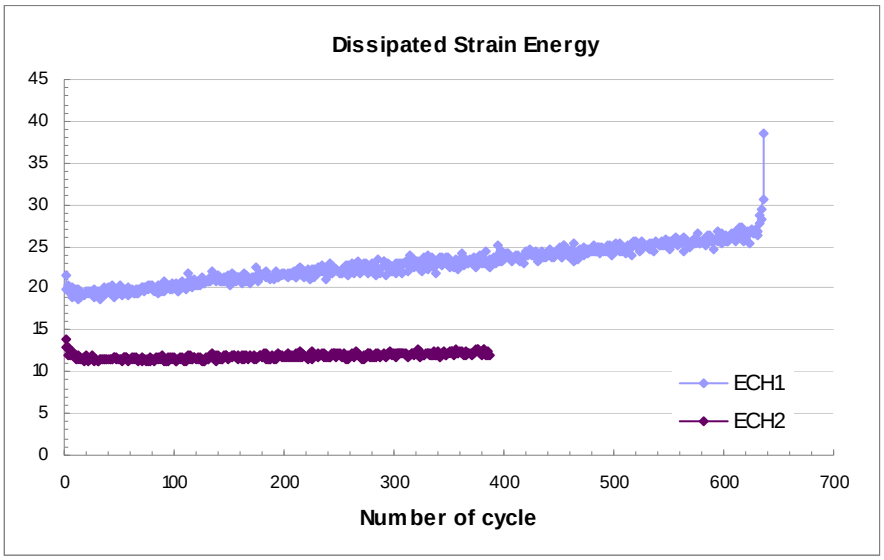

Fig. 3.6: cycles normalized area trend for ECH1 and ECH2

In conclusion, once overcome the problems given by the formulation with long glass fibres, material ECH2 shows higher properties either mechanical or fatigue behaviour.

3.3 EX materials group

As said previously, these materials are a modification of the PP-based composites commonly used by Electrolux, with the purpose of weight reduction. For this reason it is clearly very important to verify the properties of these new materials. Obviously the use of the blowing agent in the formulation will lead EX materials to show lower properties, but what it will be important to evaluate if their characteristics are enough for the applications set.

EX1 and EX2 have very similar mechanical properties, but when tested with AFT method, they revealed a different behaviour.

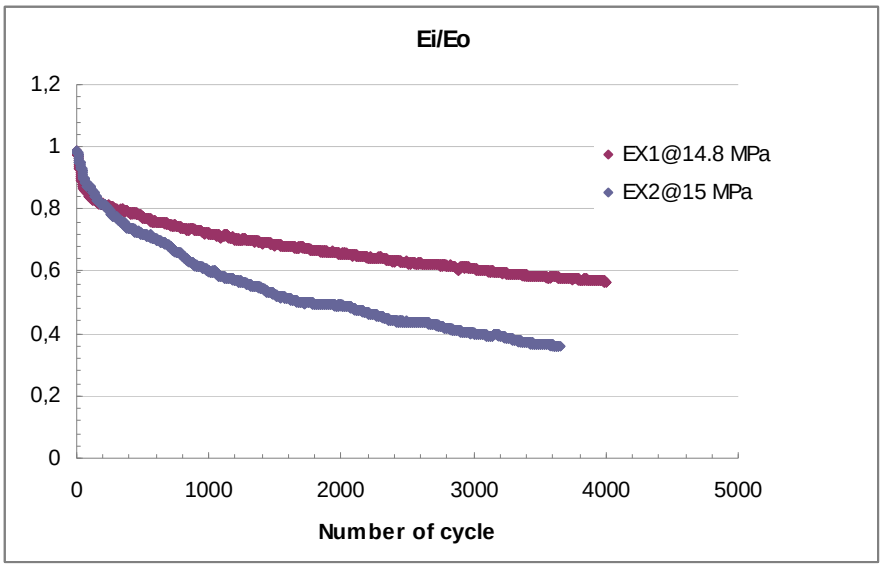

Fig. 3.7: modulus decay for EX group

The test highlights that EX1 has better fatigue properties. This fact is confirmed by the analysis of the area values, reported in the following figure.

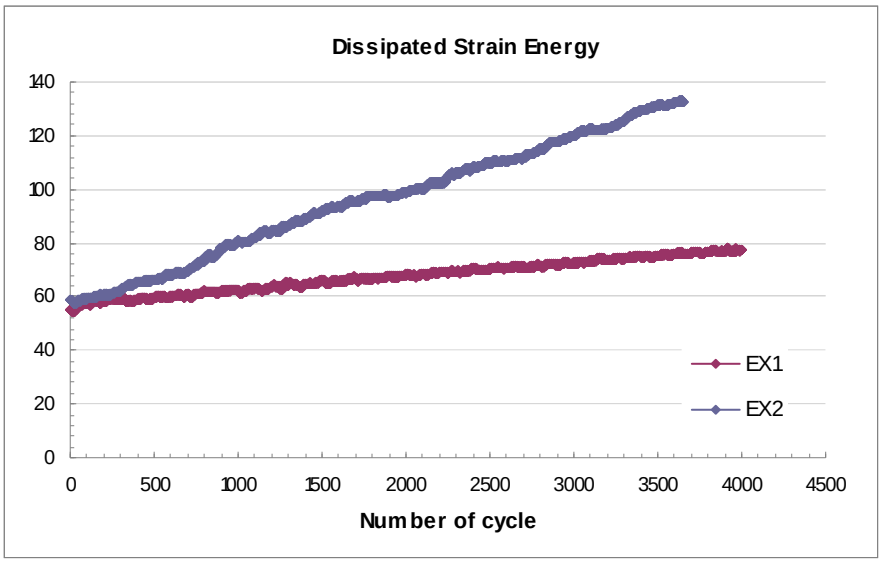

Fig. 3.8: cycles normalized area evolution for EX group

In fact also the residual strain shows as EX2 has a higher sensitivity to creep.

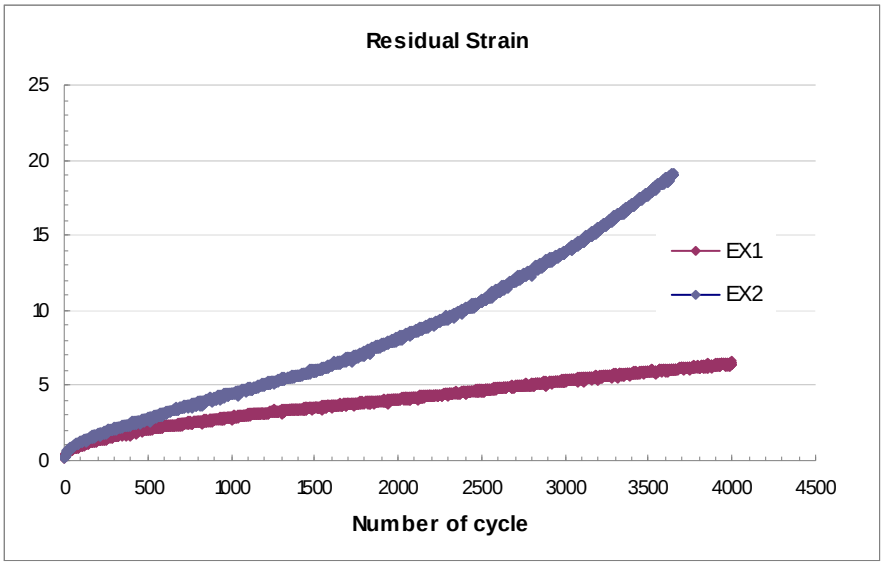

Fig. 3.9: residual strain (minimum cycle strain) evolution for EX1 and EX2

While EX1, within 4000 cycles, shows a two phases creep, EX2 denote a third phase and a strain trend towards breaking conditions.

3.4 Comparison between materials of different groups

We have seen how AFT method is able to differentiate materials with analogous formulation and with similar mechanical properties, from a fatigue behaviour point of view.

It would be interesting also compare completely different materials, in order to better understand the meaning of the parameters we have considered to evaluate damage evolution. Obviously these comparisons must be done on a normalized stress scale. First of all, the figure below shows a comparison between loading-unloading cycles for various materials.

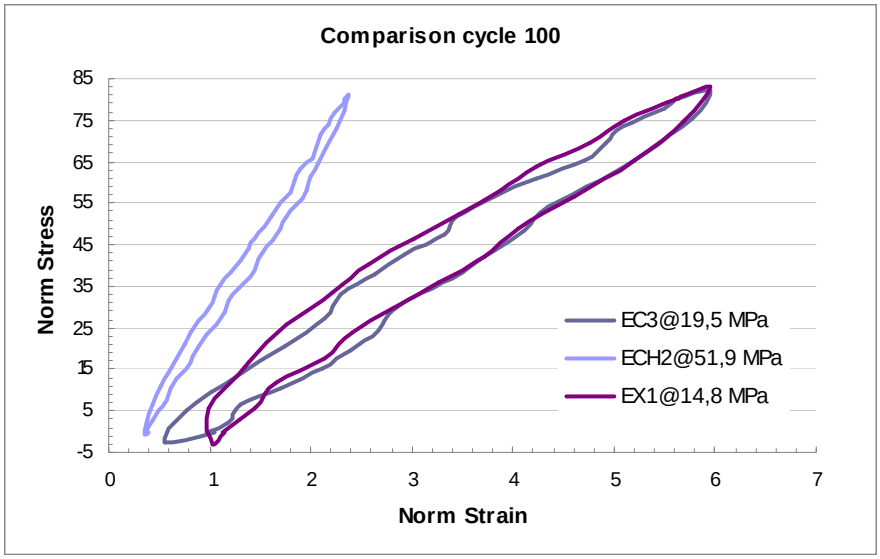

Fig. 3.10: comparison between cycle 100 shape

Figure 3.9 emphasizes the meaning of the parameters considered in the present work as indicator of fatigue behaviour. In fact after 100 cycles, is well evident as ECH1, that, thanks to the glass fibres, is much more rigid, shows an extremely lower area value (~11 Vs ~50) and, on the other hand, a

higher value of the secant modulus (~4000 Vs ~1650). On the contrary, material EC3 shows in the first part of the test, properties quite close to those of EX1. Precisely this case gives us the opportunity to differentiate the fatigue behaviour through AFT method. In the following figure the two samples are compared after 4000 cycles.

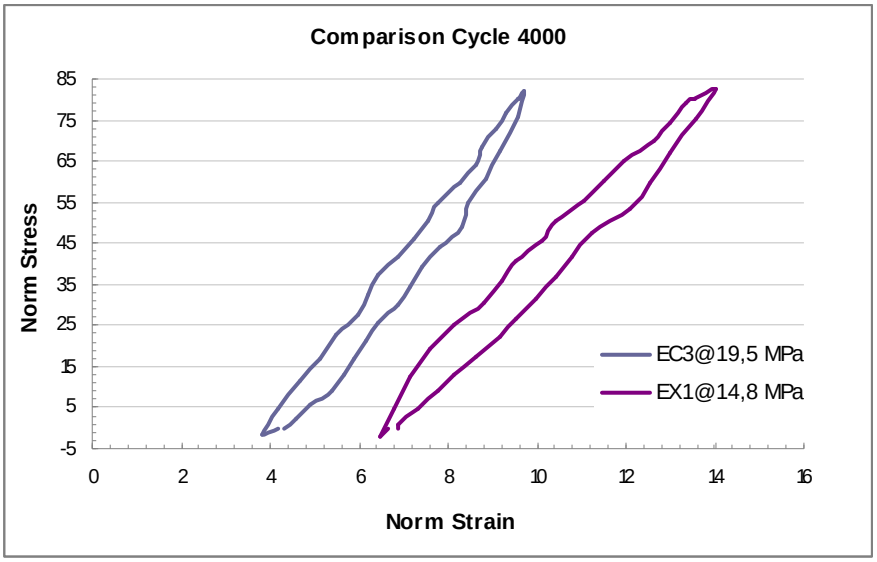

Fig. 3.11: comparison between cycle 4000 shape

It is clear how EC3 has slower evolution towards damaging conditions: higher secant modulus, smaller area and less residual strain.

For a quantitative comparison it is better to recall the plots of the relative secant modulus, dissipated energy and residual strain.

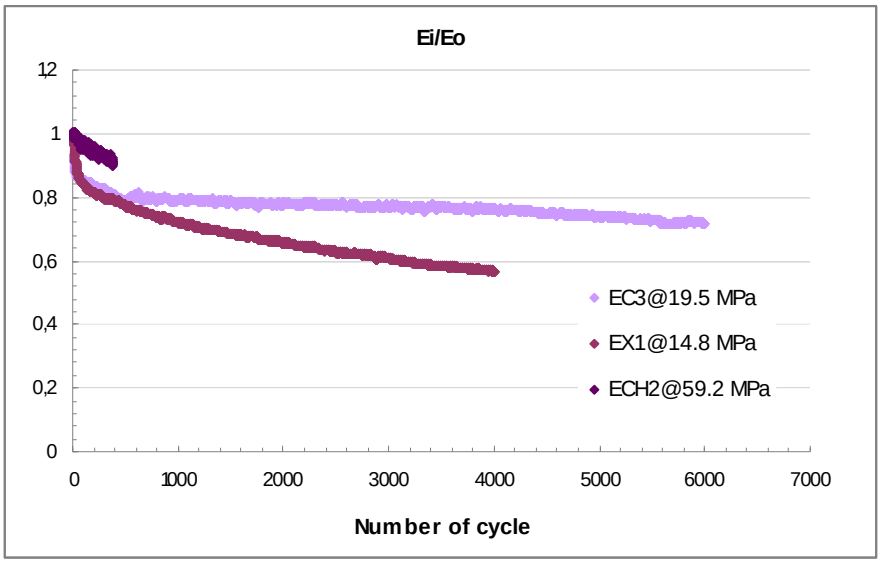

Fig. 3.12: comparison of relative modulus decay between materials of different groups

What is very interesting to underline is the different trend of E_i/E_0 between the two materials without glass fibres and ECH2 sample. As this is the only sample that breaks, its modulus trend is better fitted by an exponential rather than a power law. We have simply used the Excel trend line function, and the results are reported below.

- EC3: $y = 1.0081 * x^{-0.035}$ with $R^2 = 0.86$
- EX1: $y = 1.4696 * x^{-0.108}$ with $R^2 = 0.90$
- ECH2: $y = 0.9881 * e^{-0.0002 * x}$ with $R^2 = 0.88$

In the next chapter we will resume this matter in describing the mathematical approach to fatigue behaviour.

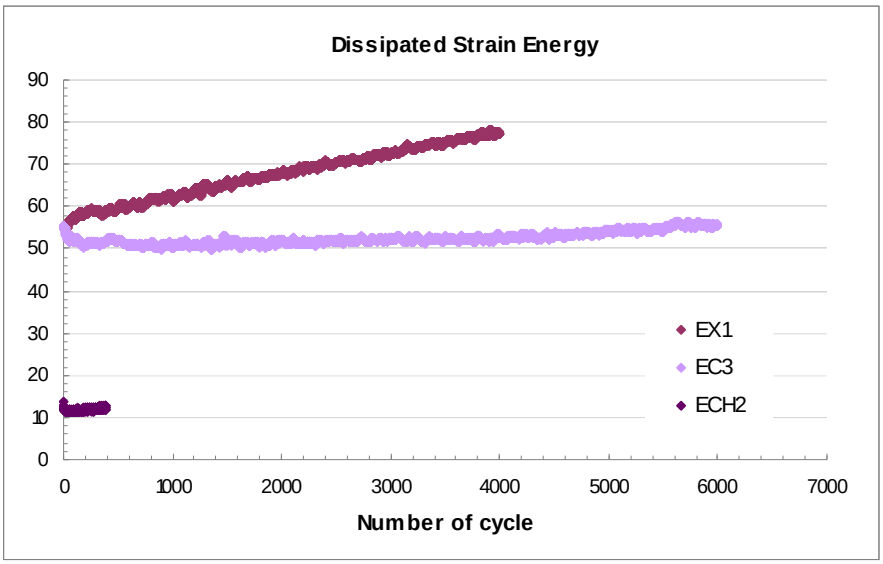

Fig. 3.13: comparison of cycles' area evolution between materials of different groups

As expected, the cycles area, being a measure of the dissipated energy, is considerably lower for ECH2 sample. About the other two samples, we have seen before that at the beginning of the test they have got comparable values, while as the number of cycles increase, EX1 shows a considerable higher damage accumulation, obviously due to its particular formulation.

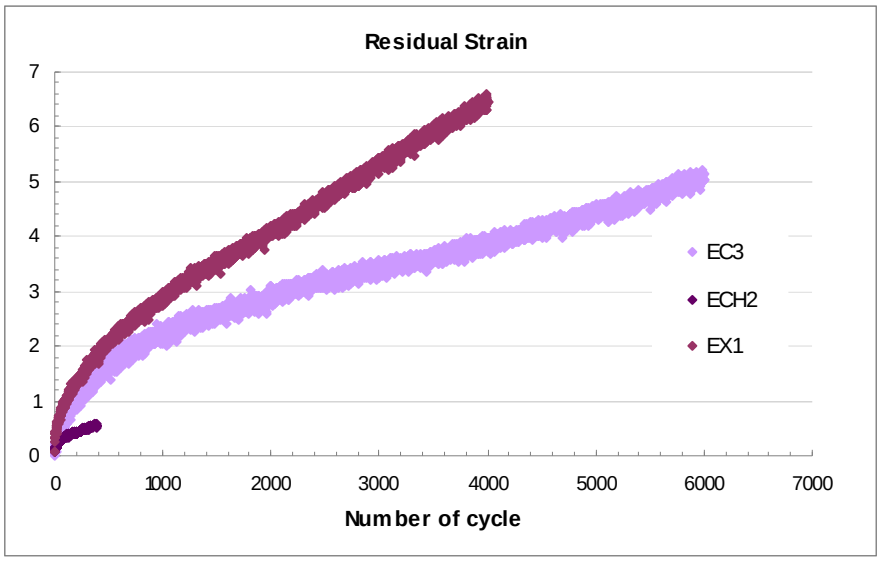

Fig. 3.14: comparison of the residual strain trend between materials of different groups

From figure 3.13 we can observe the tendency to creep of each material. As expected, ECH2 shows fewer tendencies, while EX1 has got the maximum tendency to creep.

In conclusion, in this chapter we have underlined as AFT method could be useful in characterizing fatigue behaviour, both for analogous and completely different materials. In the firs case it is possible to evaluate the effect, for example, of different matrices on the properties of a composite, situation that is very common in industrial realities, where usually a number of suppliers are taken into account. The value of the method is come out particularly in the analysis of EC and EX groups: AFT has been able to differentiate materials that resulted substantially analogous after the conventional mechanical tests. By comparing different materials we have demonstrate how AFT method could be also an academic method to get information about fatigue behaviour of thermoplastic composite materials,

and to identify from which parameters it is governed. Moreover it seems to be possible to find out a mathematical law that regulates the evolution of these parameters. In fact in the next chapter we will work out a mathematical approach able to describe the fatigue behaviour of composite materials in a general way.

4

Results simulation

As previously anticipated, the next step of the work is the development of a mathematical approach for the description of the results obtained with the AFT method. Out intention was to work out a tool able as much to describe different classes of fatigue behaviour as to predict the behaviour of a material.

Two complementary approaches have been followed. The former is a conventional mechanical approach that provides for the development of a mathematical model. The latter is a much innovative approach that consists in the development of a neural network in order to describe and predict the behaviour of materials.

In the following sections these two approaches will be described in details.

4.1 The mathematical model*

Existing fatigue behaviour mathematical models could be divided into two groups, the one containing methods developed for describing the evolution of damage parameters (i.e. the modulus trend) [1, 2, 3, 4], and the other assembling that class of methods able to describe the stress-strain hysteresis loops [5, 6, 7, 8, 9, 10].

There were two matters that forced us to develop a novel approach:

- Existing laws describing the modulus evolution gave us not enough information about the material (the shape of the loops and the area trend are essential to a complete classification of fatigue behaviour).
- Constitutive models which describe cycles' evolution have been developed for conventional fatigue test, resulting of difficult, if not impossible, implementation for our case. On the other hand all these models were based on viscoelastic considerations about the materials.

Our intention was to develop a method unconnected with materials viscoelasticity, as AFT does not provide a sinusoidal load application, but able to describe fatigue process from a macroscopic point of view, which means to work out a mathematical law that could fit the stress-strain cycles and follow damage evolution through its parameters.

* In Appendix A the method used to fit the experimental curves is reported in details

Our starting point was a model thought to describe a stress-strain curve resulting from a mechanical test on a PP-calcium carbonate-reinforced sample.

The equation describing the method is simply an exponential law and is reported below.

$$\sigma_{theor} = \sigma_y - \sum_i (\sigma_i * e^{\varepsilon / \varepsilon_i})$$

There was no doubt that an exponential law could be effective in describing the stress evolution during a tensile test on a plastic material, but the aim was to identify the physical meaning of the parameters. In this first step we hypothesized that the firs parameters could have been the value of the yielding stress, that means the higher value of stress in the linear phase of the curve, and the result of the fitting supported this assumption. On the other hand, the following terms were put in to describe the curve drop. They represent a modulus that decreases with increasing strain, in practice they are a measure of the plastic deformation of the sample. The result of the fitting is reported in figure 4.1, while the parameters value in table 4.1

σ_y	18,95115		
ε_1	0,004183		
σ_1	16,43857	σ_1/ε_1	3929,752
ε_2	0,017543		
σ_2	5,994179	σ_2/ε_2	341,6921
ε_3	0,191109		
σ_3	-4,37982	σ_3/ε_3	-22,9179

Tab. 4.7: model parameters resulting from the fitting of a tensile test on a material similar to EC1

.

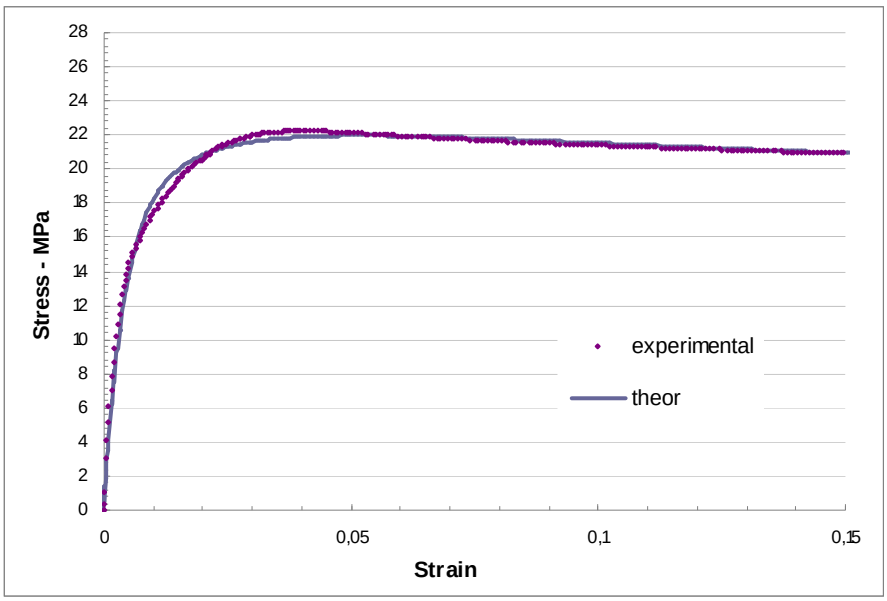

Fig. 4.15: tensile test fitted with our model (sample similar to EC1)

The data reported confirm completely the considerations made above, in fact it results that σ_y reach the value at which the curve exits the linear phase, while the σ_i / ε_i ratio, that in our intentions represents a modulus, decreases from 1 to 3.

In any case the model, with the appropriate adjustments, was used to describe the stress- strain loops. Obviously it was necessary to split the model into two equations, in order to describe the loading and the unloading phase. The modify equations are reported below.

$$\sigma_{theor} = \sigma_y - \sum_i \left(\sigma_i * e^{(\varepsilon_r - \varepsilon)/\varepsilon_i} \right) \qquad \textit{Loading phase}$$

$$\sigma_{theor} = -\sigma_m + \sum_i \left(\sigma_i * e^{(\varepsilon - \varepsilon_r)/\varepsilon_i} \right) \qquad \textit{Unloading phase}$$

where ε_r is the residual strain after each cycle, in practice the minimum value of strain for each phase. This parameter is essential to follow the shifting of the loops along the strain axis.

Before explaining the results of the fitting for the different materials from a numerical point of view, it could be interesting to illustrate, by using a figure, what we have obtained by fitting the stress-strain cycles with our model. In the figure below a discrete number of cycles (one every one thousand, from cycle 1 to 6000) for the case of material EC3, is reported.

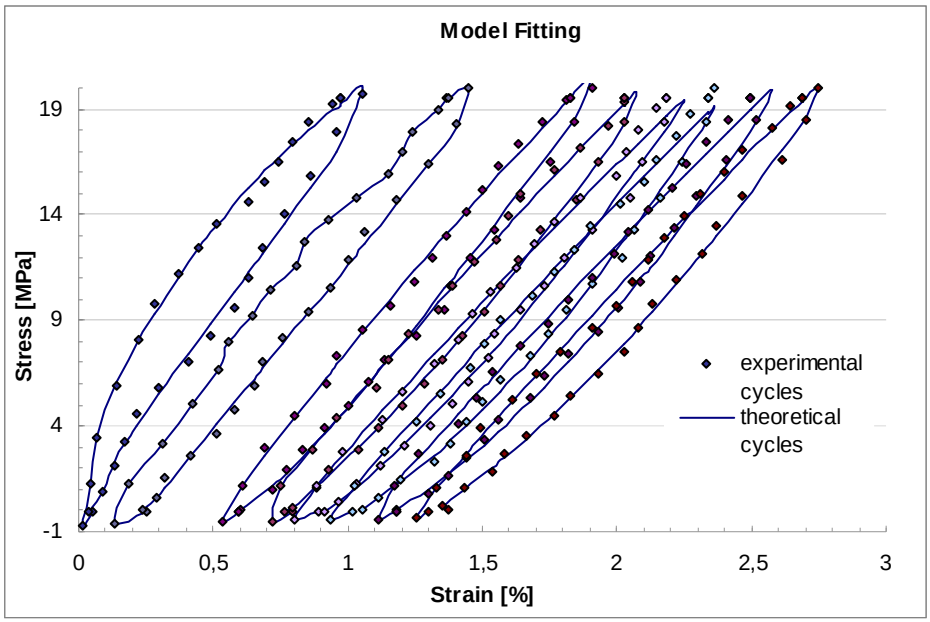

Fig. 4.16: AFT experimental data fitted with the proposed model

The figure shows as the model results are in good agreement with the experimental data, by using only one term of the summation, a part from some cycles that needed the second term to improve the fitting.

All the materials experimental results have been fitted with the model, ever by choosing a discrete number of cycles. This because at the moment we do not have at our disposal an algorithm able to manage all the

experimental data. In general also for the other materials we needed only the first term. The exceptions were represented by the first cycles, for fitting which we used also the second term. This matter derives from the nature itself of the model, in which the first term of the summation essentially describes the elastic behaviour, while the others are thought to follow the plastic deformation of the material. It is important to explain that all the samples in the first cycles showed a tendency to leave the deformation linear field, and this is represented form the initial high value of the area (see the area trend illustrated in the previous chapter). In any case it is not our intention to discuss in details this matter. For all the materials the fitting was as good as that of EC3.

As it would be boring to show how the model works on fitting a great number of cycles (in any case some examples are reported in appendix A), it is probably more interesting to focus directly our attention on a more general results. In particular after the fitting we wondered if a correlation between the parameter of the model and the material fatigue properties existed. Because of the meaning of σ_i and ε_i one idea was that their ratio could have some correlation with the secant modulus got from the test. To take into account the two phases of the model, we have study the trend of the average value between σ_i / ε_i in loading and unloading conditions. As the parameters of the second term of the summation did not showed a significant trend, and later we will try to explain why, those of the first term gave us a surprisingly result, illustrated in the following figures.

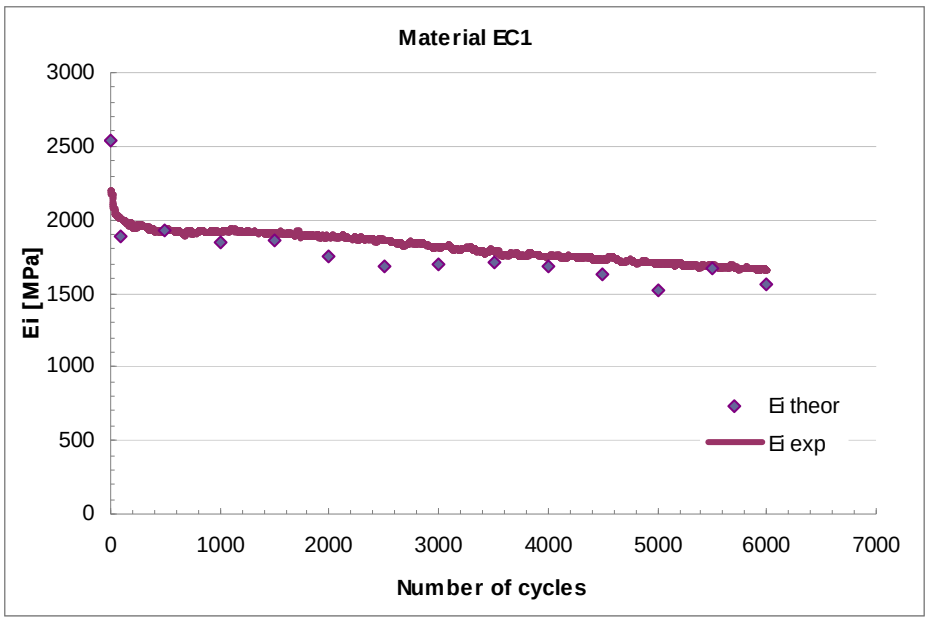

Fig. 4.17: comparison between Ei experimental data and Ei calculated with the model

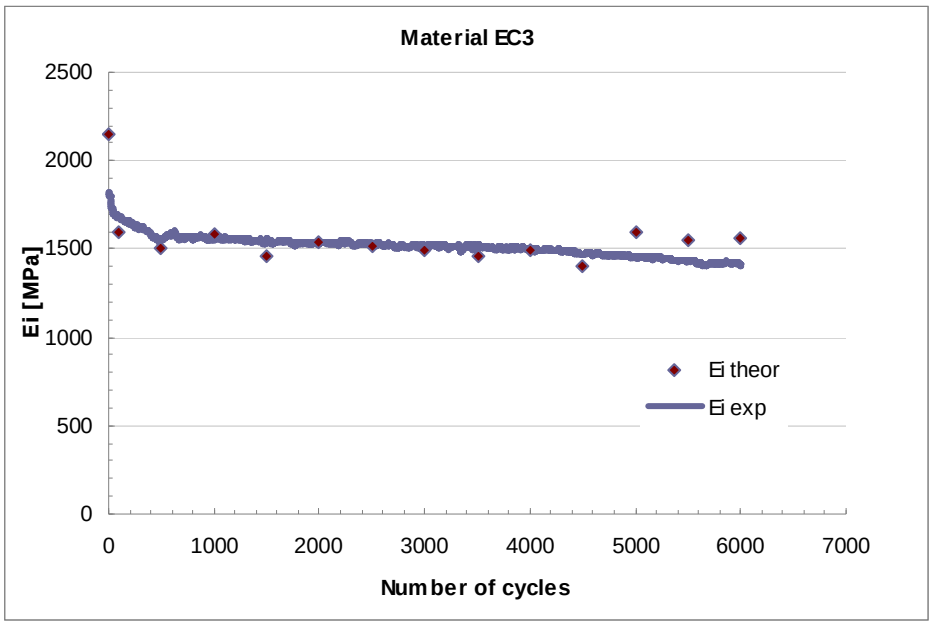

Fig. 4.18: comparison between Ei experimental data and Ei calculated with the model

It is important to underline that E_i^{theor} is the value of the ratio σ_1 / ε_1 multiplied for 100 in order to compare it with the secant modulus obtained from the test.

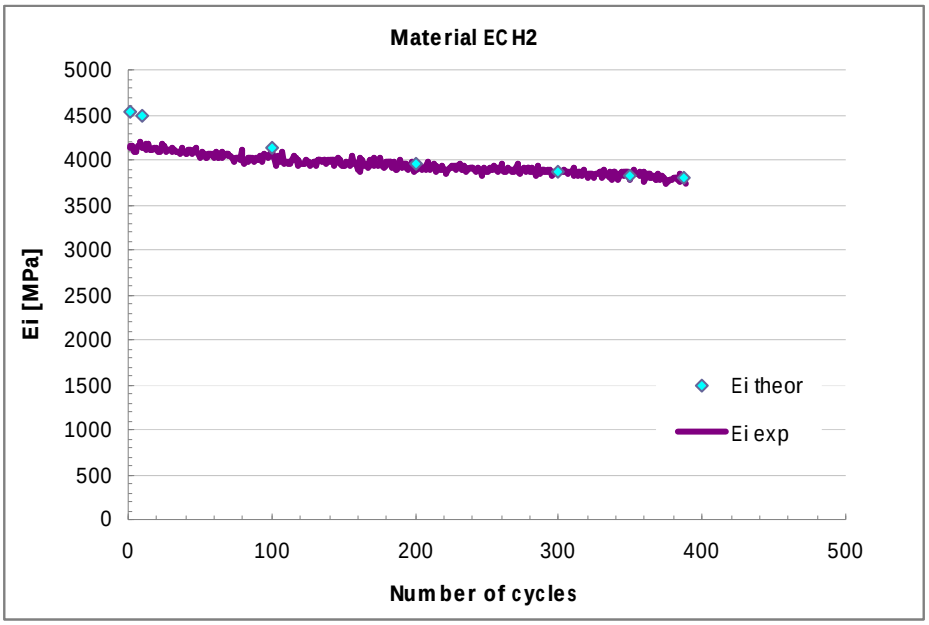

Fig. 4.19: comparison between Ei experimental data and Ei calculated with the model

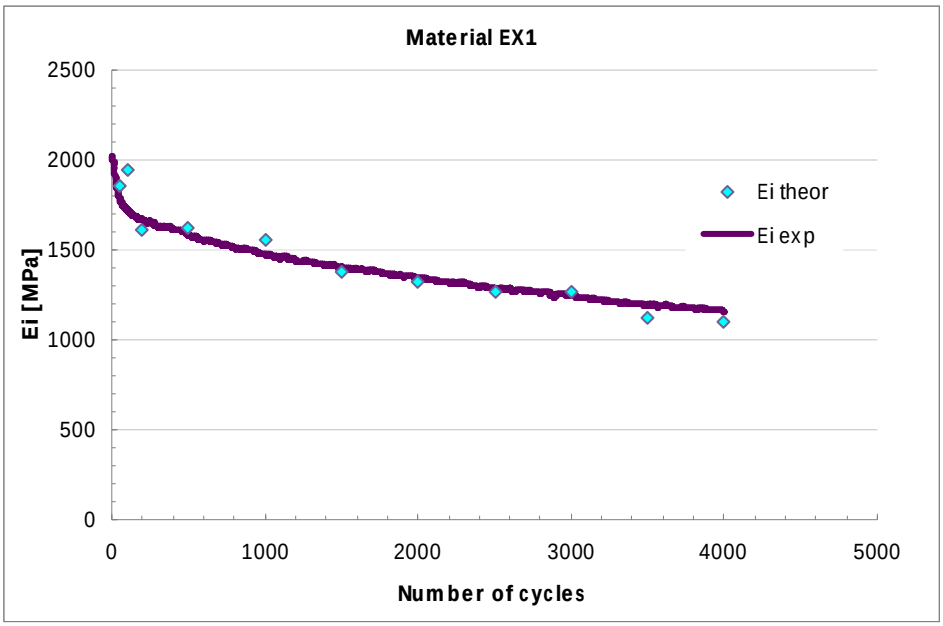

Fig. 4.20: comparison between Ei experimental data and Ei calculated with the model

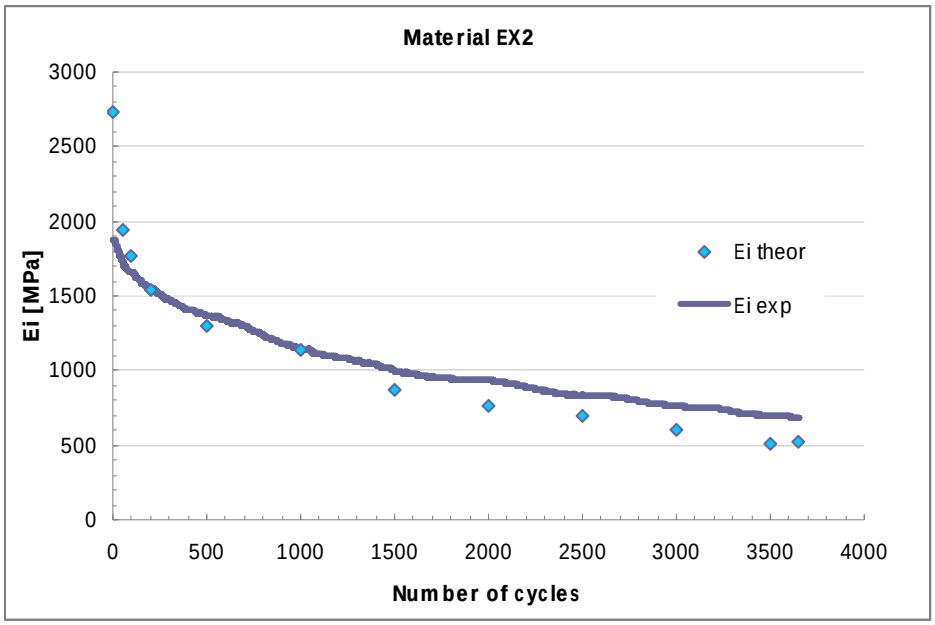

Fig. 4.21: comparison between Ei experimental data and Ei calculated with the model

The very good correlation is well illustrated in the previous figures, and moreover that correlation is valid for all the materials. This means that

the model could be really effective in the description of the material properties. On this point it is even more interesting to compare the materials from a numerical point of view. In the previous chapter we mentioned the fact that the modulus trend can be describe by a power law or by an exponential one. In particular it is essential to highlight that the latter describes materials that denote a dramatic collapse towards breaking conditions. In the following table the trend line equations for E_i^{theor} compared with those of $E_i^{\exp}$ are reported.

	E_i^{theor}	$E_i^{\exp}$
EC1	$y = 2539x^{-0.05}$	$y = 2599x^{-0.047}$
EC3	$y = 2028x^{-0.037}$	$y = 1984x^{-0.035}$
ECH2	$y = 4230 * e^{-3E-04x}$	$y = 4100 * e^{-2E-04x}$
EX1	$y = 1778 * e^{-1E-04x}$	$y = 1654 * e^{-1E-04x}$
EX2	$y = 1524 * e^{-3E-04x}$	$y = 1513 * e^{-2E-04x}$

Tab. 4.8: MS Excel trend line parameters describing Ei trends form both experimental and theoretical cases

The overestimate of the modulus value in the first cycles, leads to increase the slope of the theoretical curve in case of exponential equation, with respect to the experimental one. Apart from this, the model seems to be suitable to describe all the material groups considered in this work. In particular, it is possible to notice as it is a powerful tool to characterize different materials, even if they have similar mechanical properties. In fact the model confirms the considerations made in the previous chapter about

the materials of the three groups. Moreover the model, thanks to the good cycles fitting, can be used also to evaluate the cycle area trend.

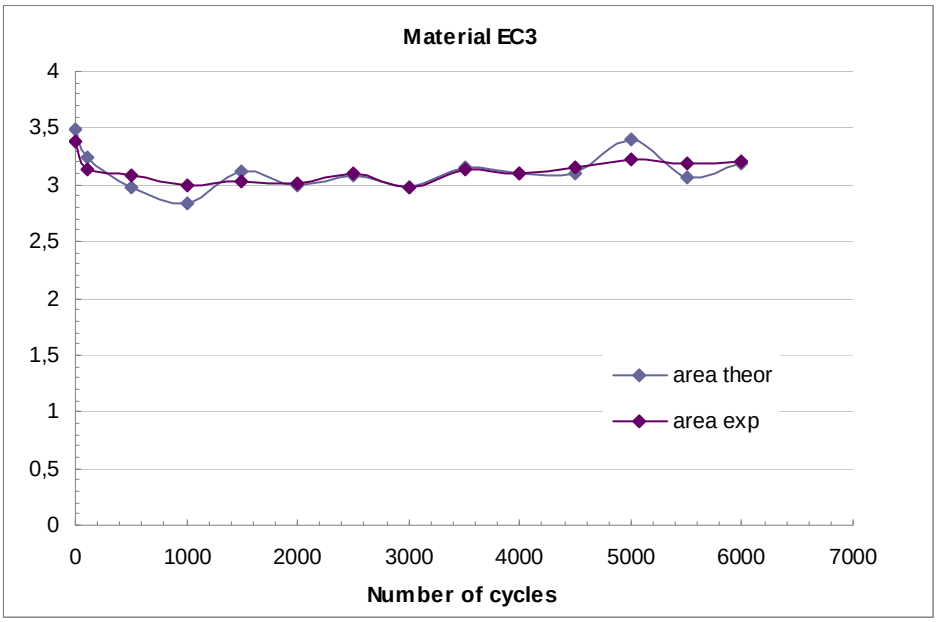

Fig. 4.22: comparison between calculated cycles area and experimental results

In the previous figure the case of material EC3 is reported, but similar results have been got with the other samples.

4.2 Final considerations about the constitutive model

In this paragraph we will try to sum up the more remarkable strength of the model and, on the other hand, to underline the unsolved points.

We have developed a mathematical model able to describe the fatigue behaviour of a vast class of materials. From a mathematical point of view, it is represented by an exponential equation. The model has at least

three adjustable parameters, but the number depends on the number of terms of summation used in the fitting. This gives to the model a high elasticity, and the possibility to describe the stress-strain curve even outside of the linear field. The ratio σ_1 / ε_1 is a measure of the secant modulus, and its trend is an indicator of the sample damaging. Moreover we found that this trend is well described by a power law for samples that do not show a high tendency to damage, while an exponential one seems to be more effective for materials that reach a high damage degree after the Accelerated Fatigue Test.

About the other terms of the summation, we did not found a significant trend, but we used it only to get a better fitting of the first cycles in some of the cases studied. On the other hand it would be important to find a significant trend for the pre-summation parameter σ_y, but to do it we would need an algorithm able to apply the model in a continuous way, that means linking the minimization process for one cycle to the result got from the previous one and so on. In fact only following this way it will be possible to propose final considerations about our model.

4.3 The neural network

As mentioned at the beginning of the chapter, we have take into consideration a second approach for the modelization of the AFT method. Actually this part of the work is still a work in progress, but we found interesting to refer briefly about the neural network approach. Before starting I would like to underline that the considerations and the results

presented below are an abstract of the Electrolux CTI workshop *"Reti neurali per la modellazione di materiali e componenti industriali"* (15/10/2008) [11, 12, 13, 14].

The peculiarity of this approach is that it disregards from constitutive details but rather implements some correlations between independent and dependent variables.

A Neural Network is an interconnected assembly of simple processing elements, units or nodes, whose functionality is loosely based on the animal neuron. The processing ability of the network is stored in the inter-unit connection strengths, or weights, obtained by a process of adaptation to, or learning from, a set of training patterns.

The Neural Networks are represented by a non linear, linked, equations system, at which some parameters are connected. The determination of these parameters enables the approximation of an experimental contest.

In particular this branch of the project examines the study of neural networks which role is the informative compression of stress-strain data got from the AFT method preformed on a plastic material sample (in this case on a material analogous to EC1). Two categories of compression codes have been considered based on different modelizations:

- Static neural network
- Dynamic neural network

In both cases the modelistic quality has been evaluated, in ex-ante and ex-post conditions. The mathematical model obtained with these methods must be considered, from an engineering point of view, like a particular codification of the constitutive mechanic equation of the material.

In mathematical terms a neural network is defined like a directional graph with the following properties:

- A state variable x_i is associated at each node or neuron
- A weight w_{ik} is associated at each connection (synapse) between two nodes *i* and *k*
- A transfer function $\sigma_i\left[x_i, w_{ik}\right]$, is defined for each node *i*. It determines the state of the node, the weights of its input connections and the state of the nodes connected to *i*. The function is assumed to be monotonic and limited.
- Nodes without input connections are referred as input node
- Nodes without output connections are referred as output nodes.
- A feed-forward network does not admit a close path, while in the present work we have considered also this case by means of dynamic neural networks.
- The size of the neural network is determined by the number of neurons and synapses.

A general example of neural network could be mathematically described as:

$$x_i(t+1) = \sigma_i\left(\sum_j \alpha_{ij} * x_j(t) + \sum_k \beta_{ij} * u_k(t)\right)$$

$$y_1(t) = \sigma_2\left(\sum_j \gamma_{1j} * x_j(t)\right)$$

Dynamic neural network

$$x_i(t) = \sigma_1\left(\sum_{j \neq i} \alpha_{ij} * x_j(t) + \sum_k \beta_{ik} * u_k(t)\right)$$

$$y_1(t) = \sigma_2\left(\sum_j \gamma_{1j} * x_j(t)\right)$$

Static neural network

The chosen of the neuron response function depends on the application studied. Once determined the kind of the function, the neural network must be trained. The training phase is the determination of the optimum for the parameters configuration, towards the comparison with a set of experimental data. In our case the error minimization has been done using an aleatory method.

Below a schematic representation of the training procedure is reported.

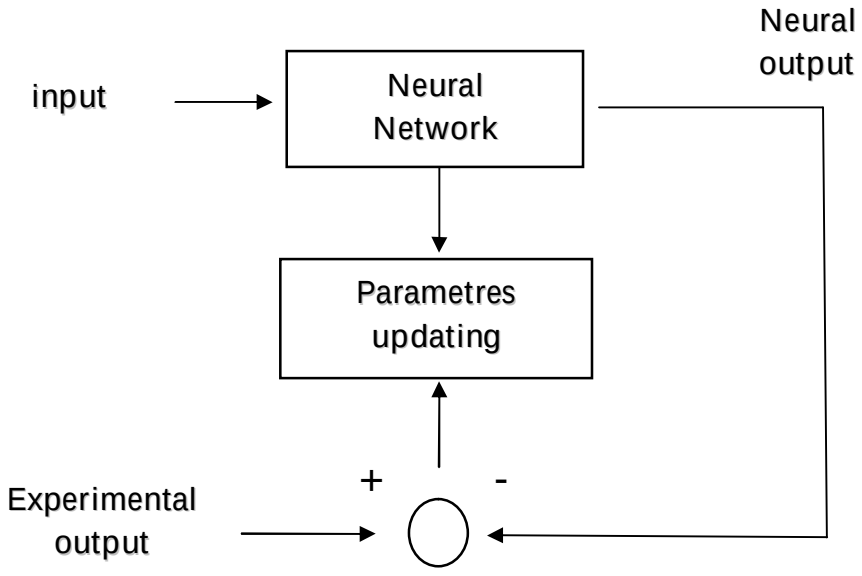

Moreover it could be advisable to compare the mathematical and the graphic representation of a 2 neuron dynamic neural network, as shown below.

$$x_i(t+1) = \sigma(\Sigma_j\, \alpha_{ij} \bullet x_j(t) + \beta_i \bullet u(t))$$

$$y_1(t) = \sigma(\Sigma_j\, \gamma_{1j} \bullet x_j(t))$$

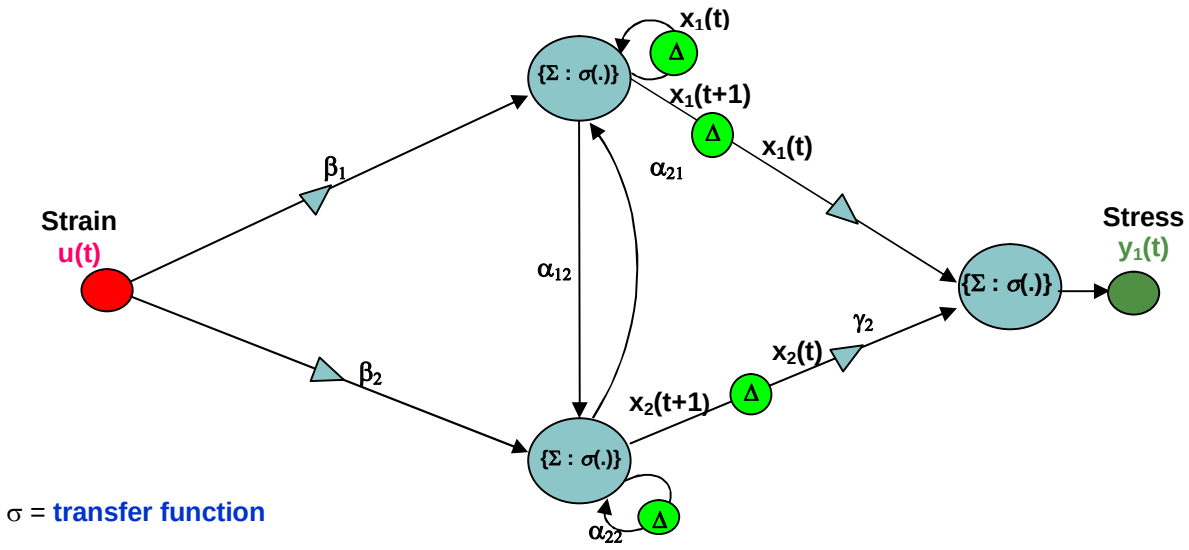

4.4 Modellization of the AFT experimental results with Dynamic Neural Networks

The aim of the activity has been the determination of a neural network model for the constitutive equations of a plastic material. The data at disposal are couples of stress-strain data obtained with the dynamometer.

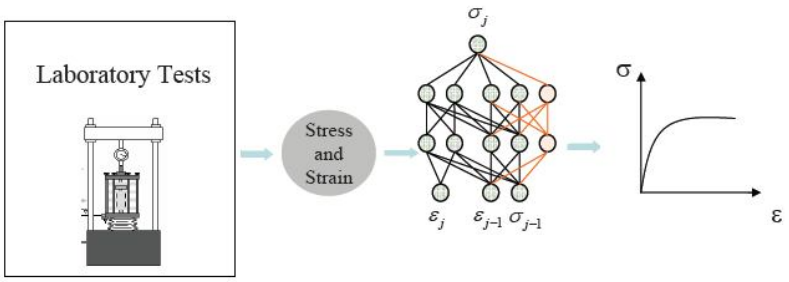

The parametric evaluation is given by the determination of the configuration $a = \{\alpha, \beta, \gamma\}$ for the minimization of the deviation between the experimental and the artificial string synthetized with the neural network.

The analytic solution of this problem is very difficult because the deviation minimization generates a non-linear equation system, which in general is transcendental and has high dimension. The better way to follow to reach the solution is to have recourse to an aleatory exploration, by using computational techniques (such as the simulated annealing).

In practice, the neural network has been determined by the minimization of the estimate error considering the first 200 cycles (4302

data). Once got the network, the forecast error has been calculated on the overall number of cycles (65500 data).

Two different kind of neural network have been compared: a radial network and a Hopfield one. Below the equation are reported.

$$x_i(t+1) = \sigma_i\left(\sum_j \alpha_{ij} * x_j(t) + \beta_j * strain(t)\right)$$

$$stress(t) = \sigma\left(\sum_j \gamma_j x_j(t)\right)$$

Gaussian σ

$$x_i(t+1) = \mu x_i(t) + \mu \sum_{i \neq j} \alpha_{ij} \sigma\left(x_j(t)\right) + \beta_i \sigma\left(strain(t)\right)$$

$$stress(t) = \sigma\left(\sum_j \gamma_j x_j(t)\right)$$

Sigmoid σ

Moreover, in both cases neural networks of different size of have been compared (5, 10 and 15 neurons). In the following figures some of the results are illustrated, while in tab. 2 the numerical results are compared.

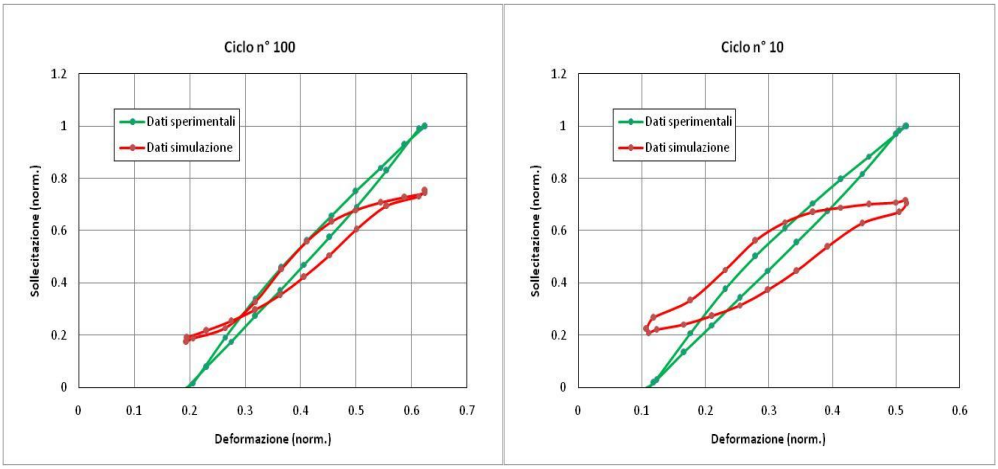

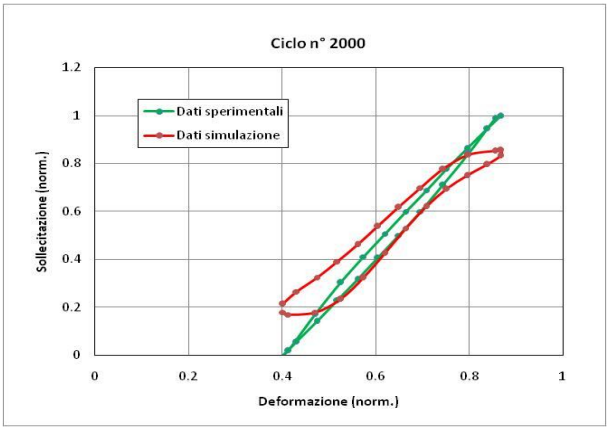

Fig. 4.23: 5 neurons Radial Neural Network after 10, 100 and 2000 cycles (estimate error = 0.03910, forecast error = 0.08616)

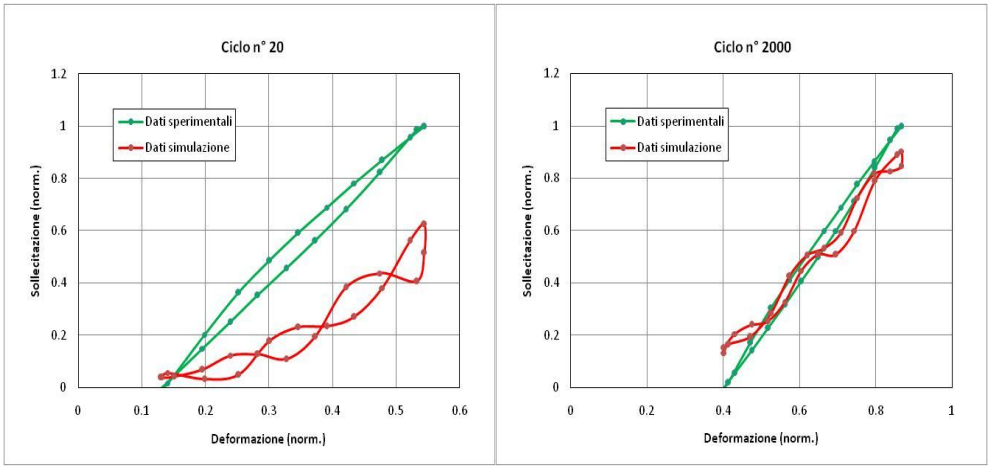

Fig. 4.24: 15 neurons Radial Neural Network after 20 and 2000 cycles (estimate error = 0.04392, forecast error = 0.10039)

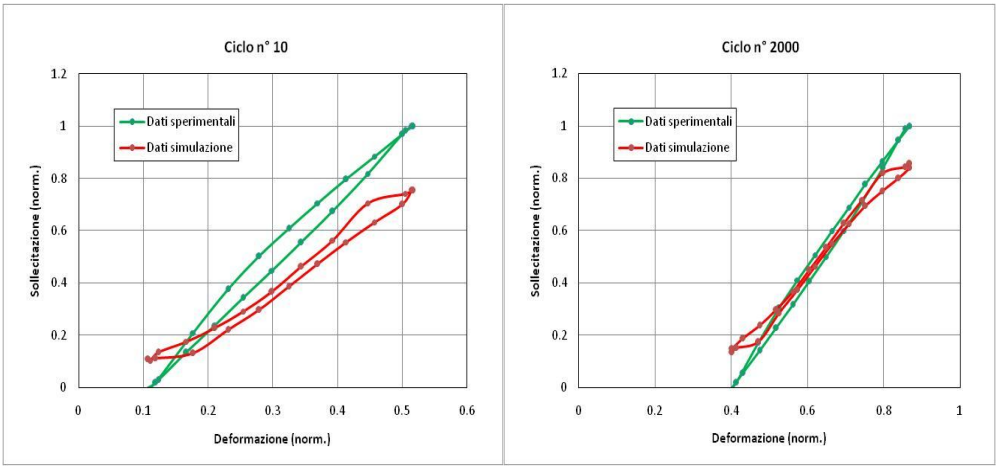

Fig. 4.25: 5 neurons Hopfield Neural Network after 10 and 2000 cycles (estimate error = 0.03218, forecast error = 0.08265)

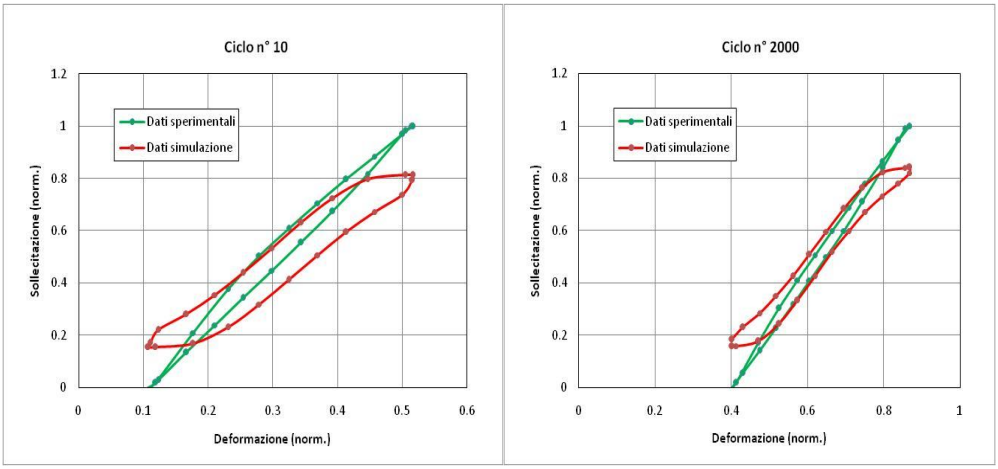

Fig. 4.26: 15 neurons Hopfield Neural Network after 10 and 2000 cycles (estimate error = 0.03596, forecast error = 0.11404)

Radial Neural Network			**Hopfield Neural Network**		
N° Neurons	Estimate Error	Forecast Error	N° Neurons	Estimate Error	Forecast Error
5	0.03910	0.08616	5	0.03218	0.08265
10	0.03595	0.10489	10	0.03415	0.09956
15	0.04392	0.10039	15	0.03596	0.11404

Tab. 4.9: comparison between estimate and forecast error based on neural network type and neuron number

In conclusion the Hopfield model results very versatile, with moderate errors in both estimate and forecast phases. Moreover, with respect to the radial model, the shape of the theoretical cycles is quite similar to that of the experimental ones.

4.5 Conclusions and further investigations

Even if in this work we have presented very shortly the Neural Networks method, it is clear that this approach has great potential in the simulation of fatigue damaging process. Moreover a good comprehension of such a kind of method could has important applications in the modellization of much more complicated situations, like, for example, the damaging investigation on mechanical structural components that undergo fatigue process. This modellization could give the possibility to estimate life endurance already in the planning phase.

For this reason the further investigation will focus from one hand on solving the open problems, like the hunting of the best method to minimize the error in the parameters configuration phase, while on the other hand it will direct to explore the possible applications effective in improving industrial productivity.

References

[1] G. Tao, Z. Xia, *Polymer Engineering and Science*, 47, 780-788 (2007)

[2] Flexural Fatigue Bahaviour of Random Continuous-Fibre-Reinforced Thermoplastic Composites", G. Caprino, A. D'Amore, *Composites Science and Technology*, 58, 957-965 (1998)

[3] Young's Modulus Degradation in Fatigue of Filled Polymers for Household Appliances, Leone C.; Caprino G., *Plastics, Rubber and Composites*, Volume 32, Numbers 8-9, October 2003, pp. 345-348(4)

[4] Fatigue model for fiber-reinforced polymer composites, H.C. Tang, T. Nguyen, T. Chiang, J Chin, J. Lesko, H.F. Wu, *Journal of Materials in Civil Engineering,* May 2000, pp. 97-104)

[5] www.ce.washington.edu/em03/proceedings/papers/519.pdf, Creep-Fatigue Interactions in Polymers, A.M. Vinogradov

[6] Cyclic deformation and relaxation characteristics in polypropylene, T. Ariyama, *Polymer Engineering and Science,* January 1993, Vol. 33, No. 1

[7] Viscoelastic-Plastic deformation behaviour of polypropylene after cyclic preloadings, T. Ariyama, *Polymer Engineering and Science,* September 1994, Vol. 34, No. 17

[8] Effect of mean strain on the cyclic deformation and stress relaxation in polypropylene, T. Ariyama, *Polymer Engineering and Science,* September 1995, Vol. 35, No. 18

[9] A constitutive theory for polypropylene in cyclic deformation, T. Ariyama, K. Kaneko, *Polymer Engineering and Science,* September 1995, Vol. 35, No. 18

[10] Cyclic deformation behaviour of an epoxy polymer. Part II: predictions of viscoelastic constitutive models, Z. Xia, X. Shen, F. Ellyin, *Polymer Engineering and Science,* 2005, Vol. 45, pp. 103-113

[11] Reti neurali per la modellazione di materiali e componenti industriali, M. Sanità, *Electrolux CTI workshop,* Porcia 15/10/2008

[12] Sistemi dinamici neurali nella modellazione dei materiali, F. Migliolo, *Electrolux CTI workshop,* Porcia 15/10/2008

[13] Il ruolo della modellazione neurale nel processo di caratterizzazione dei materiali e dei componenti industriali, F. Migliolo, *Electrolux CTI workshop,* Porcia 15/10/2008

[14] Esperimenti di modellizzazione di materiali con reti neurali dinamiche, P. Gozzi, *Electrolux CTI workshop,* Porcia 15/10/2008

5

Strain gauging method

Accurate measurement of strain, from which the stress can be determined, is one of the most significant predictors of fatigue life. Prediction of fatigue life often requires the experimental measurements of localized loads, the frequency of the load occurrence, the statistical variability of the load and the number of cycles a part will experience at any given load. A variety of methods may be used to predict the fatigue life by applying either a linear or weighted response to the measured parameters.

One of the most commonly accepted method of measuring strain is the resistive strain gage, a device whose electrical resistance varies in proportion to the amount of strain undergone by the device [1 - 7].

5.1 Strain Gage Fundamentals

Modern strain gage are resistive devices that experimentally evaluate the load or the strain an object experiences. In any resistance transducer, the resistance (R) measured in ohms is material and geometry dependent. Resistivity of the material (ρ) is expressed as resistance per unit length x area, with cross-sectional area (A) along the length of the material (L) making up the geometry. Resistance increases with length and decreases with cross-sectional area for a material of constant resistivity.

For a wire of a given length (L), resistivity (ρ) and cross-sectional area (A) the resistance (R) is given by:

$$R = \rho\left(\frac{L}{\pi/4\, D^2}\right) = \rho\left(\frac{L}{A}\right)$$

If the wire experiences a mechanical load (P) along its length, all three parameters (L, ρ, A) change and, as a result, the end-to-end resistance of the wire changes:

$$\Delta R = \left(\rho_L \times \frac{L_L}{\pi/4\, D_L^2}\right) - \left(\rho \times \frac{L}{\pi/4\, D^2}\right)$$

The resistance change that occurs in a wire under mechanical load makes it possible use a wire to measure small dimensional changes that occur because of a change in component loading. The concept of strain (ε), as it relates to the mechanical behaviour of loaded components, is the change in length (ΔL) the component experiences divided by the original component length (L).

It is possible, with proper bonding of a wire to a structure, to accurately measure the change in length that occurs in the bonded length of the wire. This is the underlying principle of strain gage. In a strain gage, the gage grid physically changes length when the material to which it is bonded changes length. In a strain gage, the change in resistance occurs when the conductor is stretched or compressed. The change in resistance (ΔR) is due to the change in length of the conductor, the change in cross-sectional area of the conductor, and the change in resistivity ($\Delta\rho$) due to mechanical strain:

$$R = \frac{\rho L}{A} \qquad \frac{\Delta R}{R} \approx \frac{\Delta L}{L} + \frac{\Delta \rho}{\rho} - \frac{\Delta A}{A}$$

The resistance strain gage is convenient because the change in resistance that occurs is directly proportional to the change in length per unit length that the transducer undergoes.

Nominal gage resistance is most commonly either 120 or 350 ohms. Higher-resistance gages are available if the application requires either a higher excitation voltage or the material to which it is attached has low heat conductivity. Increasing the gage resistance allows increased excitation levels with an equivalent power dissipation requirement.

Gage material from which the grid is made is usually constantan. The material used depends on the application, the material to which is bonded, and the control required. If the gage material is perfectly matched to the mechanical characteristics of the material to which is bonded, the gage can have pseudo temperature compensation with the gage dimensional changes offsetting the temperature-related component changes. The gage itself will be temperature compensated if the gage material selected has a thermal coefficient of resistivity of zero over the temperature range anticipated. If the

gage has both mechanical and thermal compensation, the system will not produce apparent strain as a result of ambient temperature variations in the testing environment. Selection of the proper gage material that has minimal temperature-dependant resistivity and some temperature-dependent mechanical characteristics can result in a gage system with minimum sensitivity to temperature changes in the environment.

The major function of strain gage is to produce a resistance change proportional to the mechanical strain (ε) the object to which it is mounted experiences. The gage proportionality factor, commonly called the gage factor (GF), is a fundamental parameter because it expresses quantitatively the strain gage sensitivity to strain. The gage factor is defined as the ratio of fractional change in electrical resistance to the fractional change in length (strain):

$$GF = \frac{\Delta R/R}{\Delta L/L} = \frac{\Delta R/R}{\varepsilon}$$

The gage factor for metallic strain gages is typically around 2.

5.2 Strain Gage Measurements

In practice, the strain measurements rarely involve quantities larger than a few millistrain ($\varepsilon*10^{-3}$). Therefore, to measure the strain requires accurate measurement of very small changes in resistance. For this reason strain gages are almost always used in a bridge configuration with a voltage excitation source. The general Wheatstone bridge (Fig 5.1) consists of four resistive arms with an excitation voltage, V_{EX}, that is applied across the bridge.

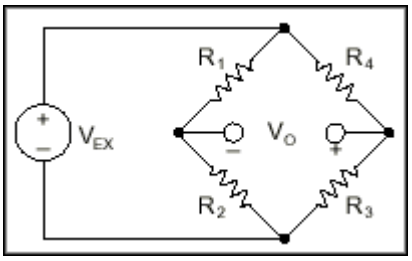

Fig. 5.27: The Wheatstone Bridge

The output voltage of the bridge, V_0, will be equal to:

$$V_0 = \left[\frac{R_3}{R_3 + R_4} - \frac{R_2}{R_1 + R_2} \right] * V_{EX}$$

From this equation, it is apparent that when $R_1/R_2 = R_4/R_3$, the voltage output V_0 will be zero. Under these conditions, the bridge is said to be balanced. Any change in resistance in any arm of the bridge will result in nonzero output voltage.

Therefore, if we replace R_4 with an active strain gage, any changes in the strain gage resistance will unbalance the bridge and produce a nonzero output voltage. If the nominal resistance of the strain gage is designated as R_G, then the strain-induced change in resistance, ΔR, can be expressed as:

$$\Delta R = R_G * GF * \varepsilon$$

Assuming that $R_1 = R_2$ and $R_3 = R_G$, the bridge equation above can be rewritten to express V_0/V_{EX} as a function of strain:

$$\frac{V_0}{V_{EX}} = -\frac{GF * \varepsilon}{4} \left(\frac{1}{1 + GF * \frac{\varepsilon}{2}} \right)$$

Ideally, we would like the resistance of the strain gage to change only in response to applied strain. However, how we have told above, strain gage material, as well as the specimen material to which the gage is applied, will

also respond to changes in temperature. Strain gage manufacturers attempt to minimize sensitivity to temperature by processing the gage material to compensate for the thermal expansion of the specimen material for which the gage is intended. While compensated gages reduce the thermal sensitivity, they do not totally remove it.

By using two strain gages in the bridge, the effect of temperature can be further minimized. For example, fig. 5.2 illustrated a strain gage configuration where one gage is active ($R_G+\Delta R$), and a second gage is placed transverse to the applied strain. Therefore, the strain has little effect on the second gage, called the dummy gage. However, any changes in temperature will affect both gages in the same way. Because the temperature changes are identical in the two gages, the ratio of their resistance does not change, the voltage V_0 does not change, and the effects of the temperature change are minimized.

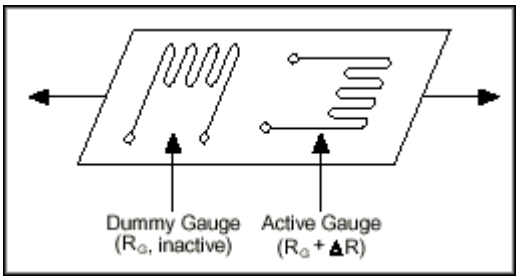

Fig. 5.28: use of dummy gauge to eliminate temperature effects

The sensitivity of the bridge to strain can be doubled by making both gages active in a half bridge configuration. For example, fig. 5.3 illustrates a bending beam application with one bridge mounted in tension ($R_G+\Delta R$) and the other mounted in compression ($R_G-\Delta R$). This half bridge configuration yields an output voltage that is linear and approximately doubles the output of the quarter bridge circuit.

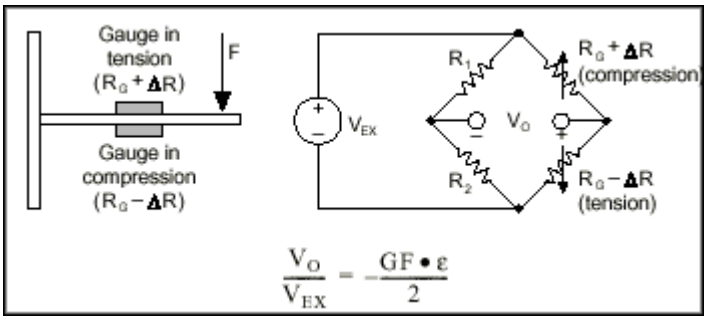

Fig. 5.29: half bridge circuit

Finally, it is possible to further increase the sensitivity of the circuit by making all four arms of the bridge active strain gages in a full bridge configuration (fig. 5.4)

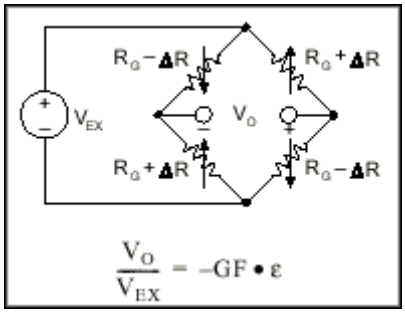

Fig. 5.30: full bridge circuit

The equation given for the Wheatstone bridge circuits assumes an initially balanced bridge that generates zero output when no strain is applied. In practice however, resistance tolerances and strain induced by gage application will generate some initial offset voltage. This initial offset voltage is typically handled in two ways. First, is possible to use a special offset-nulling, or balancing, circuit to adjust the resistance in the bridge to rebalance the bridge to zero output. Alternatively, is possible to measure the initial unstrained output of the circuit and compensate in software.

Moreover, the Wheatstone bridge equations assume that the lead wire resistance is negligible. While ignoring the lead resistance may be

useful to understanding the basics of strain gage measurements, doing so in practice can be a major source of error. One way to compensate for this error is to measure the lead resistance R_L and account for it in the strain calculations. However, a more difficult problem arises from changes in the lead resistance due to temperature fluctuations. Given typical temperature coefficients for copper wire, a slight change in temperature can generated a measurement error of several mε. Using a 3-wire connection can eliminate the effects of variable lead wire resistance because the lead resistances affect adjacent legs of the bridge. As seen in fig. 5.5 changes in lead wire resistance, R_{L2}, do not change the ratio of the bridge legs R_3 and R_G. Therefore, any changes in resistance due to temperature cancel each other.

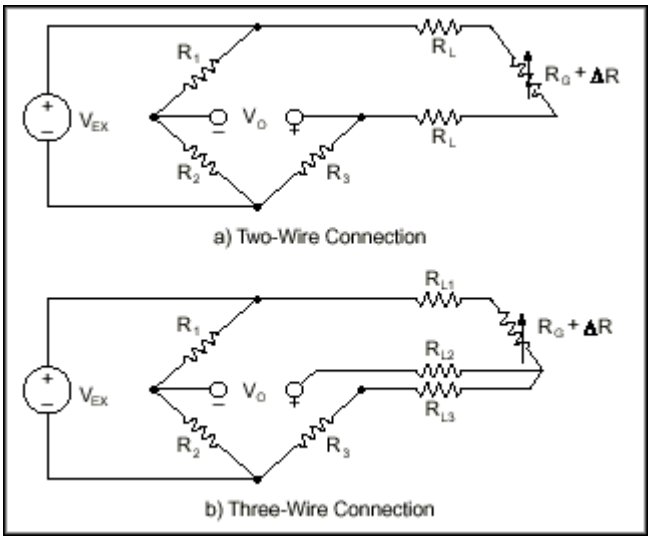

Fig. 5.31: comparison between a two-wire and a three-wire connection in a quarter bridge circuit

References

[1] www.ni.com, National Instruments web-site

[2] Short guide to Strain Gauging Methods, N. Gittins, *HBM UK Lt.*

[3] www.vishay.com, Vishay web-site

[4] La selezione dell'esetnsimetro. Criteri, procedure, consigli, *www.luchsinger.it* Luchsinger SRL web-site

[5] Previsione di vita a fatica di componenti geometricamente complessi mediante rilevazione estensimetrica delle deformazioni locali, M. T. Cascella, *AIAS, XXXI Convegno Nazionale,* 18-21 Settembre 2002, Parma

[6] Strain Gage Methods on Plastics and Composites, *www.measurementsgroup.com*

[7] Fibre breakage in polymer-matrix composite during static and fatigue loading, observed by electrical resistance measurements, X. Wang, D.D.L. Chung, *Journal of Materials Research,* Vol. 14, No. 11, November 1999

6

Strain analysis of structural components

In this chapter we will report an example of a strain analysis carried out by means of strain gauges. The component studied is a washing machine tub. This component is made of $CaCO_3$-PP microcomposite that is substantially analogous to material EC1 described previously.

The tub is the component that contains the drum. Although it is a static component, it undergoes fatigue process due mainly to two factors. The first is given by the vibration transmitted by the drum, particularly during the spinning phase, while the second is a thermal stress caused by the hot water which passes through the tub to reach the drum.

Thanks to an appropriate set up, it has been possible to evaluate the most stressed zones of the tub, the eventual presence of critical mode of the

structure, with the consequent presence of resonance, the effect of the temperature and of the load inside the machine, on the strain levels.

6.1 Strain Measurements

The strain was monitored inside and outside of the back shell. Moreover it was measured along radial, tangential and cross-sectional (45°) directions. In the following figure the strain gages set up is represented.

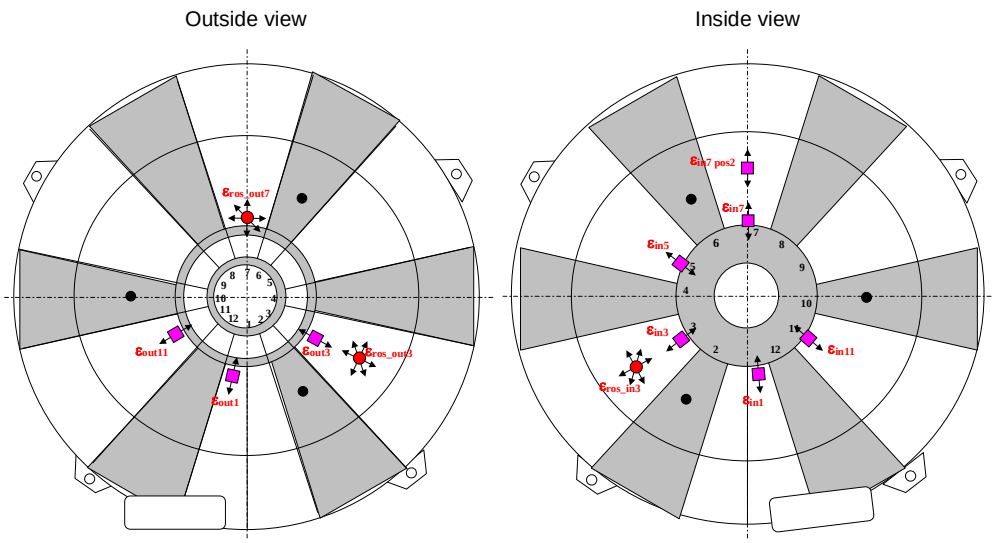

Fig. 6.32

The strain was recorded during time and as a RPM function.

About the load conditions, the strain response has been investigated on the basis of different masses applied in different positions.

Masses applied: 300 and 600g

Position considered: A (door side of the drum)

B (mass in the centre)

C (pulley side of the drum)

Cycle type: spinning (1800 RPM) and diagnostic (1600 RPM)

In the following figures, the results obtained are reported.

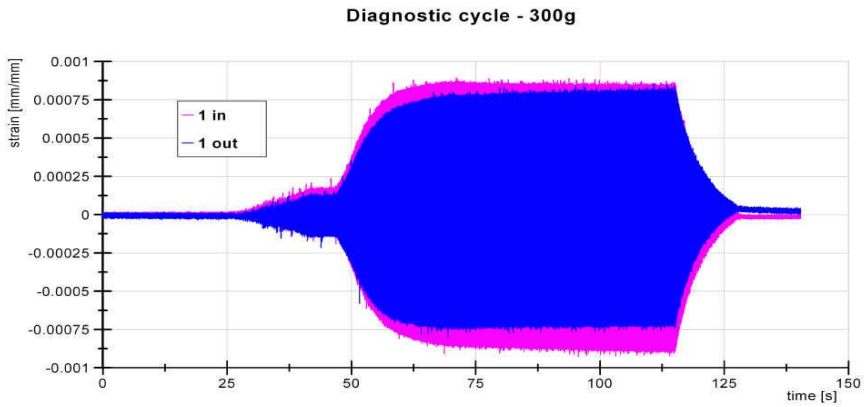

Fig. 6.33: comparison between inside and outside strain conditions (max strain achieved 0.1%)

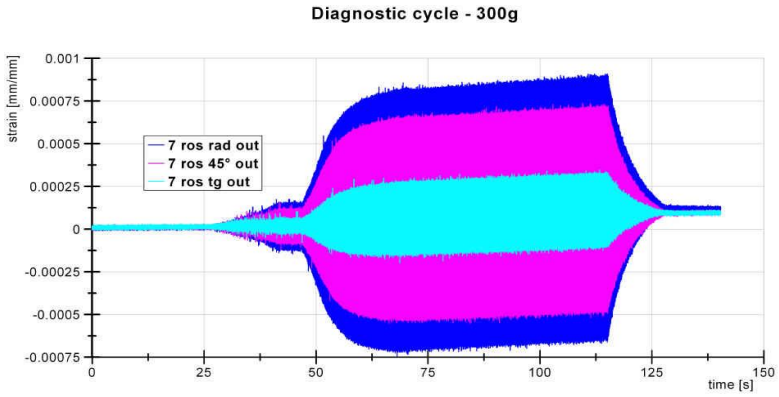

Fig. 6.34: comparison between the strain magnitudes in the three different directions

While there are no meaningful differences between the internal and external side of the back shell, the strain level in radial direction is one order of magnitude higher than in cross sectional direction and even of two orders of magnitude with respect to the tangential direction.

The data reported in the previous figures concern strain gauges close to the hub. In the following figure the zones close and far from the hub are compared.

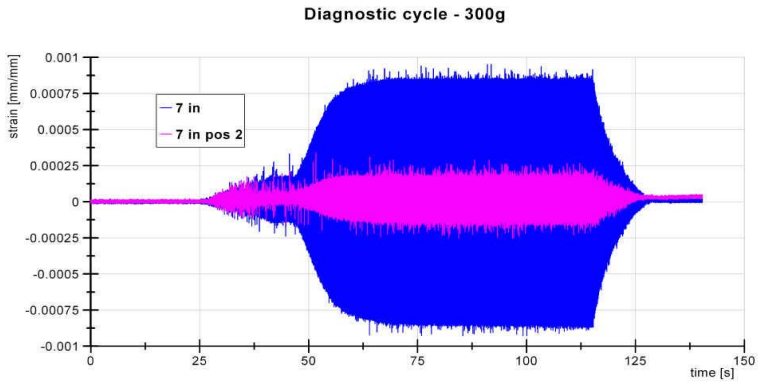

Fig. 6.35: the tub area far from the pulley zone is substantially unloaded.

In figure 6.5 the effect of the load inside the washing machine is underlined. Moreover, as the strain data are reported as a RPM function, it is possible to propose some consideration with regards to the eventual presence of critical mode.

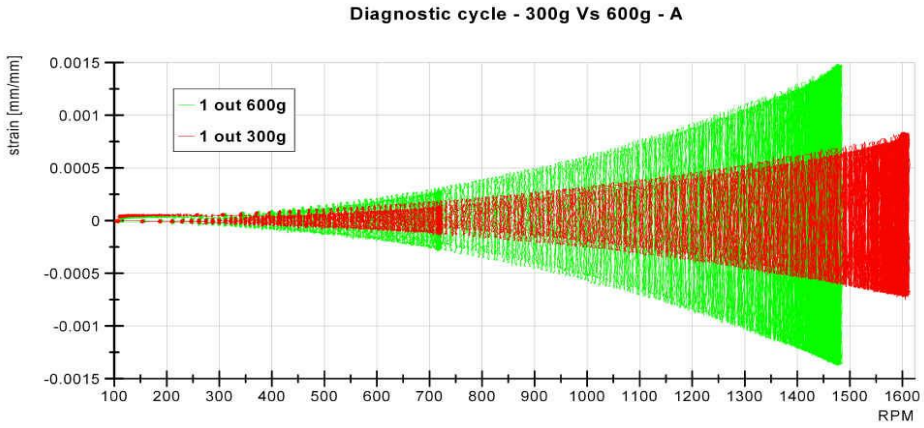

Fig. 6.36: comparison in diagnostic cycle between the conditions of 300 and 600g in position A

Even with 600g the maximum strain level is quite low (0.15%). However the 600g mass has a clear effect both on the strain level and on the engine potentiality, in fact in this case the maximum RPM was not reached. About the perfect parabolic shape of the curves, it evidences the absence of a critical mode for the structure. This fact was confirmed with the Fourier analysis, and it is true for all the load positions.

In figure 6.6 the effect of temperature is illustrated. The test at high temperature is a diagnostic cycle that follows a washing cycle at 90°C. The temperature was measured on the back shell and monitored continuously during all the phases of the test. The value reported in the figure is that at the final diagnostic phase.

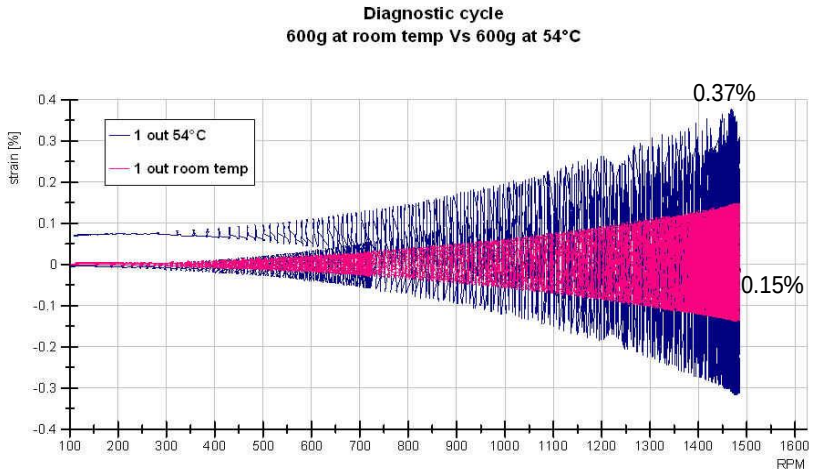

Fig. 6.37: The joint effect of load and temperature on the tub (max strain achieved 0.4% at 54°C)

Although the maximum strain level reached is not particularly high, the differences between the room temperature and the high temperature conditions are very relevant (0.4% Vs 0.15%). Moreover must be underlined the fact that at high temperature the material used tend to loose mechanical properties. Another observation that must be pointed up is the fact that, after the spinning phase at high temperature, a strain accumulation must be notice. In practice there are a drift on the time scale for the strain, meaning that not all the deformation generated by the spinning is recovered at the end of the process. This could be the effect of a creep process.

Furthermore it is important to point up some considerations about the stress level. A strain level of 0.15% for this material is generated by a stress of 6 MPa. This value is less that the 30% of the yield stress, meaning

that the structure is working with good safety margin. Nevertheless at high temperature the mechanical properties of the material change considerably and a stress value of 6 MPa does not represent anymore a safety margin or, at least, it is not more possible to consider the structure oversize.

AFT method could be, in cases like that, an effective tool to evaluate the performance of a material in operative conditions, especially if conducted even at high temperature. In fact combining strain analysis with AFT it is possible to get information the stress levels involved and to put forward considerations about the possibility to change something in the structure project or in the event of changing material or its formulation.

Conclusions and further development

In the present work a new method for the analysis of fatigue damaging of thermoplastic composite materials has been developed. The accelerated fatigue test is useful to obtain in short time information about the tendency of a material to damage (two-three hours instead of one week or more requested by conventional fatigue tests) by using a standard universal testing machine. The principal limitation of the method is given by the fact that high stress levels are needed in order to highlight in short time different trends for the damage parameters considered and compare endurance performances of various materials accordingly. The most important advantages of AFT are represented by its implementation simplicity and by its ability to differentiate in short time durability performances of materials which result very similar from the conventional static characterization. This means that AFT can become a test to be integrated with the standard characterization to support the development and the homologation of new materials formulations.

In order to interpret the experimental data, two different approaches have been considered. From one hand we have work out a constitutive model, based on a power law equation, which results effective in the description of the experimental data. Moreover a clear correlation between

the parameters of the model and the material properties has been underlined. On the other hand we followed also a completely different approach based on the neural network technique, in particular on the dynamic neural network. Although only a first set of results has been presented, this approach seems to be extremely powerful in the description of damage evolution and, as a consequence, of the simulation of life durability of the materials studied. From our point of view, the main importance of this method lies on the possibility to be implemented to the entire production process.

In the second part of the work an example of strain measurement on a structural component has been reported. In particular, thanks to strain gauging technique, a washing machine tub in operative condition has been evaluated. It appeared evident the usefulness of AFT method for a whole interpretation of the strain data. In fact the method is an important tool to a first discrimination about the structure, from points of view, design and material formulation.

With regards to the AFT method, it would be interesting to compare the results got with a conventional fatigue test. Something has been done and reported in previous works [1, 2], but those results were obtained with a different strain measurement device with respect to the video extensometer used in the present work. The way to follow to obtain a good comparison is to identify a common device for strain measurement. In particular in our opinion it must be represented by strain gauging technique, but to do it an upgrade of the instrumentation at disposal is needed.

About the model, we have mentioned that the development of an algorithm able to minimize continuously the deviation between the experimental and the theoretical data. The results we are confident to obtain are the determination of a clear trend for all the model parameters. In practice what we are confident to obtain is an instrument able to fit the experimental data starting from the variation laws of the parameters.

As told above, a great work is needed to develop the neural network method, in order to make it a crucial tool in the study of the structures damaging process.

References

[1] Experimental Study of Fatigue Behaviour of Polypropylene-Based Micro and Nano-composites, M. Basso, A. Crevatin, M. Celotto, M. Sanità, *IGF Summer School,* Trieste, July 21-24 2008

[2] A new method for the experimental study of fatigue behaviour of thermoplastic materials, M. Basso, A. Crevatin, M. Celotto, M. Sanità, *Frattura ed Integrità Strutturale,* No. 6, October 2008, pp. 20-29

Appendix A

A.1 Mechanical characterization

The term reinforcing fibres has been coined to describe discontinuous additives, the form, shape and/or surface chemistry of which have been suitable modified with the objective of improving the mechanical properties of polymer, particularly strength. Inorganic reinforcing fillers are stiffer than the matrix and deform less, causing an overall reduction in the matrix strain, especially in the vicinity of the particle, as a result of the particle/matrix interface. Reinforcing fillers are characterized by relatively high aspect ratio of length to diameter for a fibre, or the ratio of diameter to thickness for platelets and flakes. For spheres, which have minimal reinforcing capacity, the aspect ratio is unity. A useful parameter for characterizing the strengthening effectiveness of a filler is the ratio of surface area, A, to its volume, V, which needs to be as high as possible for effective reinforcement.

In this work all the materials contain discontinuous reinforcements: glass fibres with high aspect ratio and $CaCO_3$ particles with low aspect ratio.

The mechanical characterization of the prepared materials was carried out on the injection moulded test samples accordingly to the following standards:

- Flexural properties: ASTM D 790 – “Standard Test Method for Flexural Properties of Unreinforced and Reinforced Plastic and Electrical Insulating Materials”.
- Tensile properties: ASTM D 638 – “Standard Test Method for Tensile Properties of Plastics”.

From the tensile tests the following tensile properties were determined:

- Tensile yield stress [MPa]
- Tensile yield strain [%]
- Tensile stress at break [MPa]
- Tensile strain at break [%]

On the other hand the flexural tests were carried out to determine the flexural modulus [MPa].

A.2 The mathematical model

Although the results of the mechanical model have been described previously, it is opportune to give more details about the implementation of the model itself on the experimental data.

At the moment, the only way to develop the fitting is to manage cycle by cycle. The model has been applied to every single cycle, by the help of MS Excel Solver. In practice the model parameters determination has been conducted with the method of the minimum squares, by minimizing the following object function:

$$O.F. = \sum_{i=1}^{n} \left(1 - \frac{F(x_i)_{calc}}{F(x_i)_{\exp}} \right)^2$$

obtained by the sum of the relative squared deviations.

Actually not all the cycles have been fitted, but a choice has been done. We chose a sample of cycles that is one every one thousand.

In the following table some examples of the parameter values obtained for different cycles and different material are reported.

MATERIAL EC1 - LOADING PHASE								
n	**σy**	**σ1**	**ε1**	**σ1/ε1**	**σ2**	**ε2**	**εr**	**O. F.**
1	28,4085	26,49587	0,845308	31,34464	0,555763	0,004876	0,0156	0,004465
100	71,67621	69,66504	3,421853	20,35886	0,708071	0,004393	0,1322	0,00931
500	71,22891	70,119	3,357149	20,88647	-0,1411	0,004393	0,24	0,010451
1000	77,40025	76,31772	3,787273	20,1511	0	0	0,3123	0,040539
1500	83,27789	82,19281	4,105443	20,02045	0	0	0,3832	0,028571
2000	56,05928	54,96559	2,710499	20,27877	0	0	0,4064	0,006455
2500	63,30746	61,94102	3,234405	19,15067	0	0	0,4414	0,007615
3000	63,78209	62,91792	3,258863	19,30671	0	0	0,4662	0,00709
3500	63,9729	62,72314	3,245896	19,32383	0	0	0,5137	0,00716
4000	64,13383	62,62338	3,454148	18,12991	0	0	0,5382	0,017323
4500	116,3632	115,0321	6,709242	17,14532	0	0	0,5538	0,005447
5000	116,4248	114,9414	7,13266	16,1148	0	0	0,5672	0,020043
5500	116,4688	114,9083	6,919756	16,60584	0	0	0,6172	0,008361
6000	116,5698	114,7879	7,180542	15,98597	0	0	0,641	0,01341

MATERIAL EC1 - UNLOADING PHASE								
n	**σy**	**σ1**	**ε1**	**σ1/ε1**	**σ2**	**ε2**	**εr**	**O. F.**
1	129,6625	131,1817	6,785601	19,33236	-0,82901	-0,01324	0,0723	0,002992
100	75,39207	76,16635	4,375425	17,40776	0	-0,01324	0,1935	0,008618
500	76,87519	77,43861	4,35353	17,78754	0,566809	-0,00806	0,3278	0,018372
1000	77,33031	76,95382	4,58548	16,78206	0	0	0,3293	0,035592
1500	76,91468	77,37084	4,499994	17,19354	0	0	0,4491	0,06638
2000	77,67924	79,90381	5,426168	14,72564	0	0	0,502	0,012831
2500	77,96877	79,62437	5,442551	14,62997	0	0	0,5146	0,009431
3000	77,98407	79,62627	5,464647	14,57117	0	0	0,5743	0,027676
3500	78,16548	79,45747	5,317264	14,9433	0	0	0,5989	0,010882
4000	78,60246	79,02862	5,094155	15,51359	0	0	0,5906	0,227527
4500	78,5467	79,0779	5,16633	15,3064	0	0	0,6266	0,181846
5000	78,51945	79,05446	5,569362	14,19453	0	0	0,6357	0,019433
5500	74,71032	70,38141	4,21245	16,70795	0	0	0,6516	0,022104
6000	79,35559	77,08291	5,051875	15,25828	0	0	0,6857	0,010549

The results got from the other materials are substantially analogous in terms of O. F. values. Also the requirement of the second term of the

summation to fit the first cycles is a constant matter for all the cases studied. Moreover, if the parameter σ_2 is not used, it would be not necessary to use two different parameters σ_y and σ_1. In fact it emerged another link between the parameters, that is $\sigma_y \approx \sum_i (\sigma_i)$. In any case we chose to use two different parameters with the purpose of a better fitting.

Although a law governing σ_y and σ_1 trend does not emerge, we are confident that this fact is due to the fitting process followed. In fact probably the minimum for the O.F. lies on the plan generated by the couples of σ_y and σ_1 values that origin a determined value for σ_1 / ε_1. This means that by imposing a law for the pre-exponential parameters, it would be possible to fit all the experimental cycles. As told previously, a software able to do this is developing.